Acta Materialia 241 (2022) 118386

Contents lists available at ScienceDirect

Acta Materialia

journal homepage: www.elsevier.com/locate/actamat

Full length article

In situ observation of atomic-scale processes accomplishing grain rotation at mixed grain boundaries

Yizhong Guo[a], Jiao Teng[b], Guo Yang[a], Ang Li[a], Yao Deng[c], Chengpeng Yang[a], Lihua Wang[a,*], Xin Yan[c,*], Ze Zhang[d], Xiaoyan Li[e], En Ma[a,f], Xiaodong Han[a,*]

[a] Beijing Key Lab of Microstructure and Properties of Advanced Materials, Beijing University of Technology, Beijing, 100124, China
[b] Department of Material Physics and Chemistry, University of Science and Technology Beijing, Beijing, 100083, China
[c] School of Mechanical Engineering and Automation, Beihang University, Beijing, 100191, China
[d] Department of Materials Science, Zhejiang University, Hangzhou, 310027, China
[e] Center of Advanced Mechanics and Materials, Applied Mechanics Laboratory, Department of Engineering Mechanics, Tsinghua University, Beijing 100084, China
[f] Center of Alloy Innovation and Design (CAID), State Key Laboratory for Mechanical Behavior of Materials and School of Materials Science and Engineering, Xi'an Jiaotong University, Xi'an, 710049, China

ARTICLE INFO

Article history:
Received 15 October 2021
Revised 12 September 2022
Accepted 25 September 2022
Available online 26 September 2022

Keywords:
Atomic scale
Dislocation
Grain boundary plasticity
Plastic deformation
In situ transmission electron microscopy

ABSTRACT

A detailed monitoring of atomic-scale processes accomplishing grain rotation is important for understanding the deformation mechanisms in nanocrystalline metals. However, direct observations have been rare thus far, such that our knowledge about grain rotation has to rely heavily on hypothetical models and simulations. Here, we present in situ atomic-resolution evidence, indicating that the atomic processes accomplishing grain rotation in nanocrystalline Pt depend on the type of grain boundary (GB) separating the rotating grains. The grains around general (mixed) GBs rotate via the Frank–Bilby dislocation activities together with atomic shuffling and disconnection activities, the former being the generation, climb, glide and reaction of GB dislocations, whereas the latter leading to GB migration accompanying the grain rotation. While for the grains with a tilt GB in between: their rotation is accomplished almost entirely via the Frank–Bilby dislocation activities. We also discover that the GB dislocation climb, glide, and reaction often involve the formation and destruction of Lomer-like dislocations.

1. Introduction

Grain rotation, i.e., a change in the misorientation angle between adjoining grains, is one of the most important processes in plastic deformation, especially for nanocrystalline (NC) metals at room temperature when the grain size is less than ~15 nm [1–6]. Stress (strain)-induced grain rotation has been confirmed in experiments by several groups [4,7–16]. However, what is actually happening to the atoms mediating and accommodating the rotation remains unsettled, as a real-time atomic-scale observation is highly challenging. At present, the understanding of the atomistic mechanisms behind grain rotation relies largely on classical models and simulations [7,17–27]. The model developed in the 1950s [23,24] by Frank and Bilby proposed that grain boundaries (GBs) actually consist of Frank–Bilby dislocations. Many studies have extended this model and proposed that grain rotation occurs via the absorption/generation of a Frank–Bilby dislocation in the GB without obvious GB migration. For example, Li et al. suggested that the dislocations in GBs will be removed or added under shear stress, which will change the density of GB dislocations at GBs, thus leading to grain rotation and growth even at low temperature. Because the absorption/generation of a Frank–Bilby dislocation mainly occurs in the GB, grain rotation occurs without obvious GB migration [21]. Ovid'ko et al. [22] and Murayama et al. [28] proposed that grain rotation can be explained through the disclination model. This disclination consists of arrays of dislocations at the GBs, and the movement and climb of an individual dislocation will lead to grain rotation and structural change of the disclination. During this process, the plasticity that mainly occurs at the GB involves short-range diffusion, which induces minimal GB migration. However, there is no direct experimental evidence supporting this. In addition to the model of grain rotation without the need of GB

* Corresponding authors.
E-mail addresses: wlh@bjut.edu.cn (L. Wang), yan_xin@buaa.edu.cn (X. Yan), xdhan@bjut.edu.cn (X. Han).

https://doi.org/10.1016/j.actamat.2022.118386

migration, there are also many other theoretical models, which purport that grain rotation is always accompanied by GB migration. The classical theory, the Ashby–Verrall model, proposed that grain rotation occurred during the deformation [25]. This grain rotation will lead to both compressive and tensile strained regions around the GB, setting up long-range diffusion from the former to the latter. This mass transport via long-range atomic diffusion is necessary to accommodate the rotation and also leads to shape change (or GB migration) of the grains [18,25]. A previous theoretical model and molecular dynamic (MD) simulation proposed that the GB migration accompanying grain rotation can occur via disconnection glide [29,30]. The disconnections have both step and dislocation character (Burgers vector b and step height h). The glide of GB disconnection shifts the GB atom-columns, and the GB atom-columns that belong to one side become part of another side, which shifts the two crystals by b (parallel to the GB) and migrate the GB by h (normal to itself). In the meantime, the disconnection shear on the GB bounding a grain will also induce a torque that leads to grain rotation [17,29,30]. This disconnection gliding results transformations of the structural units between the GB and grain lattice, without the need for long-range diffusion [29,30]. Although many grain rotation models have been proposed, it is unknown which of the aforementioned grain rotation mechanisms is valid under experimental conditions, particularly in the new scenario of NC metals. In several experiments, the postmortem transmission electron microscopy (TEM) examinations indicate that in grain rotation via GB dislocation activities, the GB migration can be negligible during the rotation process [28,31–34]. However, other studies have suggested that GB migration is always coupled with grain rotation [8–10]. These two mechanisms have to be reconciled. Thus, direct experimental evidence with atomic resolution is needed to resolve this issue.

In this work, we perform tensile experiments inside a high-resolution transmission electron microscope (HRTEM) to monitor the atomic-scale dynamic processes underlying grain rotation in NC Pt [35–37]. We provide direct evidence that the operating mechanism depends on the type of GB involved in grain rotation. This conclusion was further corroborated via molecular dynamics simulations. Specifically, grains separated by a tilt GB can accomplish their rotation via GB dislocation absorption/generation,glide, and climb at GB with negligible GB migration. While the rotation of grains separated by mixed GBs [38,39] is carried by a combined activation of GB dislocation activities (glide and climb at GB), as well as atomic shuffling and disconnection activities that mediate concurrent GB migration. Our findings thus reconcile previous different classical models. We also report a hitherto unnoticed behavior - the reactions between climbing and gliding dislocations in the GB frequently form Lomer-like dislocations that is subsequently destructed during deformation-driven grain rotation.

2. Experimental and simulation methods

2.1. In situ TEM tensile device

The TEM extensor was made of two thermally actuated bimetallic strips. They were fixed, in opposing positions, on a TEM Cu-ring grid using superglue or epoxy resin, as the schematic view shows in Supplementary Figure. 1a. Each bimetallic strip was made of two layers of two different materials that have a large mismatch in their thermal expansion coefficients to achieve a significant deflection at relatively low operation temperatures. The conventional TEM specimen holder (hot stage), now with the bimetallic strips fabricated, can therefore act as a double-tilt, displacement-controlled deformation stage. The elevated temperature (below 80 °C) was expected to have a minor impact on the room-temperature GB deformation mechanisms that we studied, given the high melting point of Pt at 1768 °C.

2.2. Transferring thin film specimens to the uniaxial tensile devices

Operated under optical microscope, the bimetallic extensors (two metallic bars) can be well aligned to be vertical to the thin film samples as shown in Supplementary Fig. 1a, 1b. Using epoxy resin on the surfaces of the bimetallic extensors, the thin films can be attached on the surface of the extensors in almost ideal geometrical configuration, as shown in Supplementary Fig. 1b. Thus, the uniaxiality of the deformation can be ensured during the loading process. Etching away NaCl single-crystal substrate with water, free-standing bimetallic strips, together with thin film tensile samples, were released from the NaCl substrate as shown in Supplementary Fig. 1c. Then, the bimetallic strips with the attached thin films were loaded onto the TEM-tensile stage. Later, with TEM observation, the temperature controller could accurately increase the temperature of the TEM-tensile stage and the bimetallic extensor exerted uniaxial tensile force on the thin films, as shown in Supplementary Fig. 1d The dynamic process could be recorded accordingly, either by digital CCD camera or the negative films.

2.3. Molecular dynamic simulations

To further reveal the deformation mechanism of grain rotation, we constructed a polycrystalline Pt thin film sample with length, width, and thickness equal to 65, 40, and ~ 8 nm, respectively. The sample consisted of 101 grains and 1.3 million atoms with a mean grain size of ~ 6 nm. A U-shaped edge notch was created with a tip radius of 5 nm and a length of 15 nm that similar with previous MD simulation [26]. We used Atomsk package [40] to create the initial atomistic structure and the visualization was realized with OVITO package [41]. When building this model, we first created a 2D Voronoi tessellation using Atomsk [40]. The grains with out-of-plane orientations were randomly selected to mimic our experiments. Our model contained 101 grains, and there are 279 mixed GBs and 9 tilt GBs. In this model, we also can see that many of these GBs are irregular shapes. We performed molecular dynamics simulations of loading process of a polycrystalline Pt nanofilm using LAMMPS [42] with an embedded-atom method (EAM) potential [43]. To generate realistic GBs, we equilibrated the entire system at room temperature for 200 ps at the initial stage of simulations. After equilibration, the sample was stretched in the length direction. The step-loading was adopted in this simulation [26,44]. In every loading step, a 5 ps equilibration was performed after the system was stretched for 5 ps at the strain rate of 10^8 s^{-1}. We repeat this loading-equilibration cycle until the sample is stretched to the strain of 10%. Thus, the average loading rate in our simulation is less than 10^8 s^{-1}. The equilibration after every small loading period gives the dislocation a period of time to move. This provides us the possibility to capture dislocation glide/climb at the interface. During the simulation, the temperature was controlled at 300 K with Berendsen thermostat. Atoms at the two ends of the length direction in the sample were fixed during loading. To measure the grain rotation, a specified marker (around 1.5 nm in length) at the center of the grain (there was no defect created in the marker area during loading) was selected. The rotation of the marker was calculated to represent the rotation of the grain.

3. Results

Pt thin film samples for in situ TEM straining experiments were prepared using magnetron sputtering. The film thickness is about ~ 15 nm and most of the grain sizes are less than ~ 10 nm in size, as is shown in Fig. 1a. The selected area diffraction pattern of the

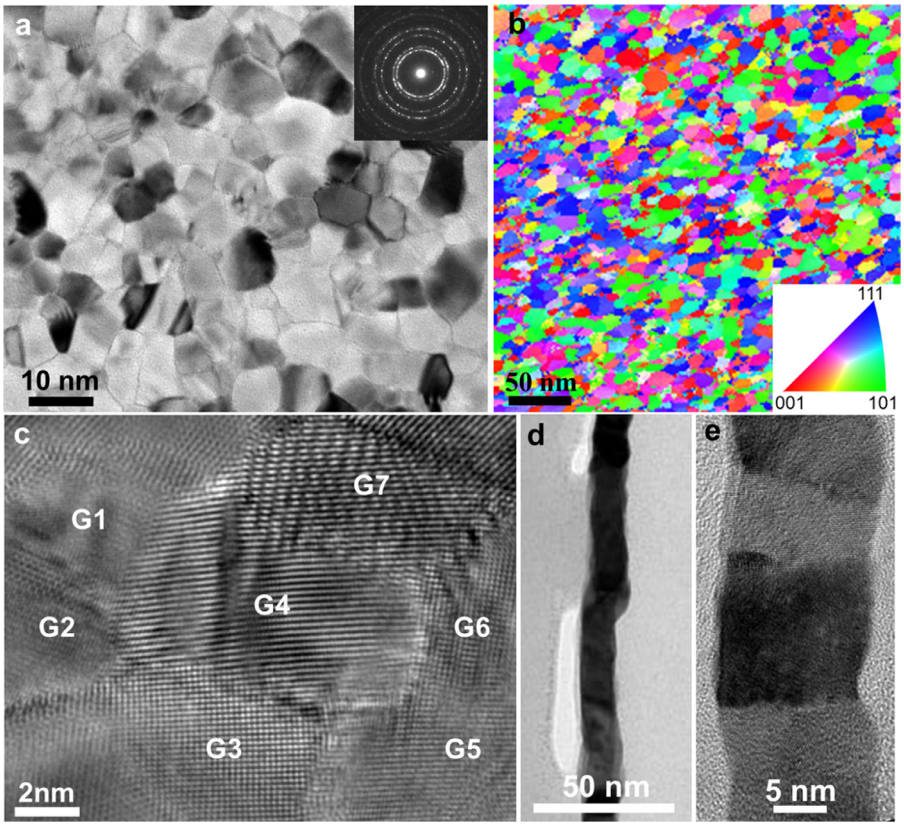

Fig. 1. (a) Typical TEM image which presents the Pt film has nanometer-sized and equiaxed grains, with no obvious texture, consistent with the selected area diffraction pattern of the thin film inserted in Fig. 1a. (b) A typical inverse pole figure image acquired from the precession electron diffraction analysis. (c) HRTEM image which shows that most grains are separated by high-angle GBs, without visible porosity or micro-cracks. (d) Low magnified cross-sectional TEM image of the thin film. (e) Enlarged TEM image which reveals that the thin film has only one grain in the thickness direction that can serve as a columnar microstructure.

thin film is shown in Fig. 1a. The continuous diffraction ring reveals that the nanograins randomly distributed without a preferred orientation. This is further confirmed by the inverse pole figure image acquired from precession electron diffraction analysis (Fig. 1b). As can be seen, most of grains are surround by others in different crystal zone axes and the GB is curved. This indicated the rotation axis varies for different regions of the GB, thus, most of the grains are obviously separated by mixed GBs according to previous theories [45]. To further confirm the types of the GBs, a HRTEM image is taken in Fig. 1c where most of the grains surrounding the G_4 are in different axial lattices and the shapes of most of the GBs is curved, indicating the GBs are belong to mixed GBs. The thin film sample has a columnar microstructure with one grain in the thickness direction, see cross-sectional TEM images in Fig. 1d, 1e. In the current study, the orientation relationship between two grains can be roughly determined from the lattice or fringe images. Our large number of HRTEM examinations show that a few of two nearby grains are in the same axial lattices, and most of the grains surrounded by others are in different axial lattices. In addition, the GBs in NC are highly curved because of the small grain size (small size indicating large curvature of GBs). The in situ straining experiment was performed using a custom-made tensile testing device (see Supplementary Fig. 1 and Supplementary Materials for details) inside a JEOL-2010 field emission HRTEM operating at 200 kV. The applied strain rate is in the range of $10^{-3} \sim 10^{-4}$/s.

3.1. Atomistic mechanisms of mixed grain boundaries during grain rotation in experiment

In this paper, the term "tilt rotation" refers to the in-plane rotation about the normal direction of the film plane, and the term "twist rotation" refers to the out-of-plane rotation about a direction in the film plane; the symbol $GB_{i\text{-}j}$ denotes the GB between two adjoining grains G_i and G_j; the misorientation angle of $GB_{i\text{-}j}$ refers to the angle of in-plane rotation between grains G_i and G_j. Fig. 2a–c display a series of HRTEM images to demonstrate the grain rotation. The double-ended arrow in Fig. 2b indicates the direction of the applied tensile load, which produces a torque to drive the rotation of the grains. From the images in Fig. 2a–c, we see that grains G_1 and G_4 exhibit no appreciable changes in their lattices during the in-situ straining, indicating negligible global rotation and tilt of the specimen. Note that the observed fringes in these grains are not Moiré fringes because only a single grain is present in the thickness direction of the film owing to the columnar grain microstructure. The fringes in the grains can be well indexed with the FCC lattice of Pt. Enlarged HRTEM images are presented in Fig. 2d–g. Specifically, as observed in Fig. 2d, G_1 exhibits the $[01\bar{1}]$ axial lattice in this projected view, whereas G_4 exhibits the [001] axial lattice. In addition, $GB_{1\text{-}4}$ is irregularly shaped/curved. From this information, $GB_{1\text{-}4}$ should be a mixed GB. To track the grain rotation, we monitored the angle between the edge-on (111) plane of G_1 and the edge-on (100) plane of G_4 from the fast Fourier transform (FFT) images. Fig. 2h–k show the combined FFT images taken from the red framed regions of G_1 and G_4 that correspond to those in Fig. 2d–g, respectively. From Fig. 2h–k, both the (111) and (100) planes can be well indexed, and thus, the grain rotation can be well monitored by measuring the change in angle between these two planes. As noted in Fig. 2h, the measured angle between the (111) plane of G_1 and the (100) plane of G_4 is ~20.1° Upon straining, the angle increases from ~20.1° to 26.5° (Fig. 2j) and subsequently to 28.7° (Fig. 2k). Along with this clear grain rotation, the nearly hexagonal G_1 changes its shape, and

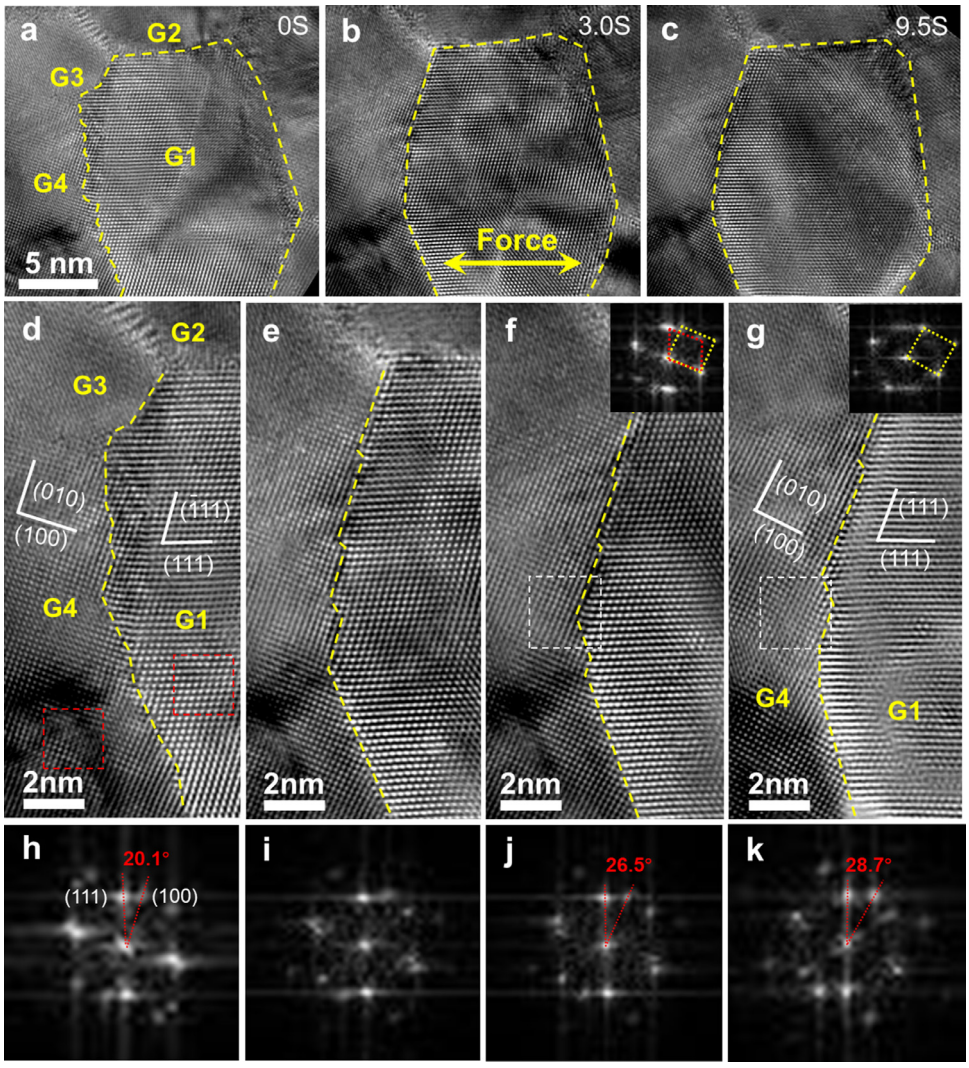

Fig. 2. In situ HRTEM images showing grain rotation. (a–c) The grain G_1 undergoes rotation during an in situ straining experiment. During grain rotation, the shape of G_1 changes slightly, indicating the occurrence of GB migration. (d–g) Four enlarged HRTEM images showing the atomic structures near the GB of GB_{1-4} during grain rotation. G_1 exhibits the $[01\bar{1}]$ axial lattice, while G_4 exhibits the [001] axial lattice. Hence, GB_{1-4} is a mixed GB. The FFT images inserted in (f, g) were taken from the white framed regions. (h–k) The combined FFT images taken from the red framed regions of G_1 and G_4 corresponding to those in (d–g), respectively. The angle between the edge-on (111) plane of G_1 and the edge-on (100) plane of G_4 increases from ~ 20.1° to 26.5° and then to 28.7°

the GB_{1-4} (yellow dashed lines in Fig. 2d–g) changes its morphology significantly with local GB segments obviously migrating toward the G_1 side. This is also confirmed by the FFT images (shown in the insets) taken from the same region (corresponding to the white framed region of Fig. 2f and g). As noted in Fig. 2f, the two sets of spots, with square and parallelogram shapes, indicate that both the $[01\bar{1}]$ and [001] axial lattices exist in the white framed region. As grain rotation, as shown in Fig. 2g, there is only one set of spots with square shape in the FFT image, indicating that GB_{1-4} migrates toward the G_1 side, and thus only the [001] lattice exists in the white framed region. Such a migration of the GB in between rotating grains is a hallmark feature of the grain rotation that involves long-range mass transport or glide of disconnection (disconnection model) [25,26,29,30].

More details about the grain rotation accompanying with GB migration are illustrated in Fig. 3, which presents a series of enlarged HRTEM images from the same in situ experiment (Fig. 2). Fig. 3a shows an HRTEM image in the early stage of grain rotation. The red arrows 1 and 2 point to the local regions without an atomically abrupt interface between the adjoining grains G_1 and G_4. This "gradual" interface arises because the lattice planes of grains G_1 and G_4 locally have a nearly perfect match in this projected view across the GB_{1-4}. During grain rotation, the edge-on (111) planes in G_1 near the red arrow 1 switch, smoothly over a few planes, to the edge-on (100) planes in G_4, as seen in Fig. 3b and c, resulting in GB migration in this local region. Meanwhile, in a nearby region of the red arrow 1, an atomically sharp interface separates G_1 and G_4, disallowing the smooth switching from (111) planes to (100) planes. Instead, the migration of this GB_{1-4} segment entails more local shuffling and/or short-range atomic diffusion to reach the atomically sharp interface between G_1 and G_4 seen in Fig. 3d. By comparing the lattice near the GB_{1-4} in Fig. 3a-d, the GB migration is obviously dominated by the (111) planes in G_1 switching to the (100) planes in G_4, rather than obvious long-range diffusion. Thus, we believe this grain rotation should be governed by disconnection model [29,30], which accomplishes concurrent GB migration. The GB migration can be understood in terms of the nucleation and motion of disconnections with Burgers vector *b* (the component of b parallel to the GB plane) and step-height *h*. The glide of a disconnection shifts the two crystals by *b* parallel to the GB and migrate the GB (normal to itself) by *h*. In the meantime, the disconnection shear on the GBs bounding a grain will

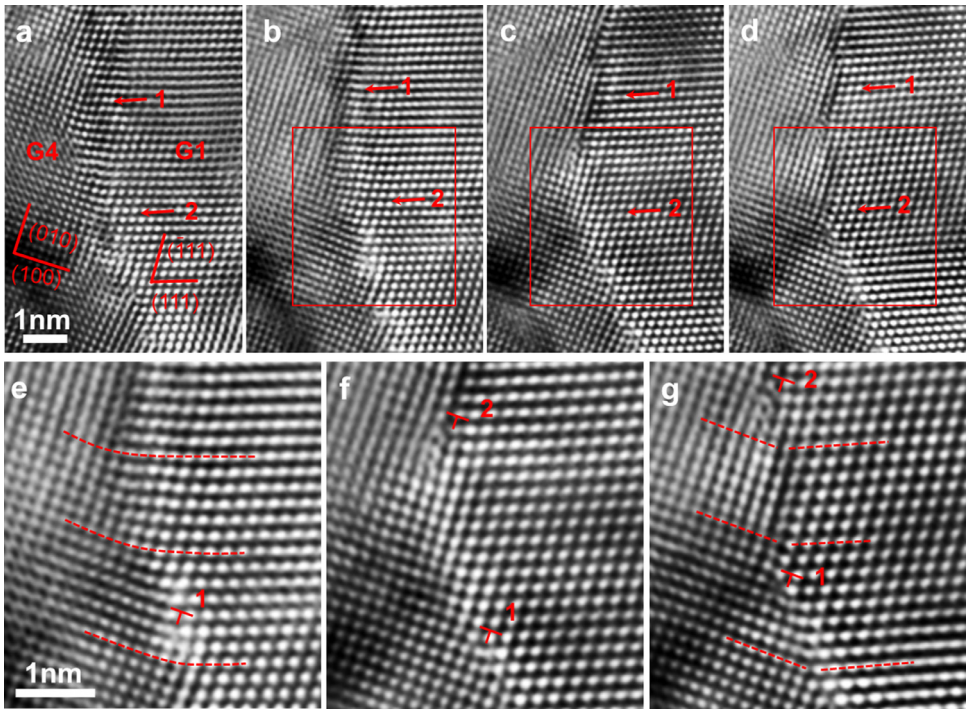

Fig. 3. In situ observation of a mixed GB migration as well as the dislocation generation and climb at this GB during grain rotation. (a) An HRTEM image captured at the early stage. As indicated by red arrows 1 and 2 near GB_{1-4}, the edge-on (111) planes in G_1 are continually switched to the edge-on (100) planes in G_4. (b, c) During the grain rotation, the (111) planes of G_1 near the upper part of GB_{1-4} become the (100) planes of G_4 (as indicated by red arrow 1), resulting in the marked GB migration. (d) With further rotation, the shuffling of the GB atoms leads to the structural change of GB_{1-4}, so that the interface between G_1 and G_4 becomes atomically sharp. (e–g) Enlarged HRTEM images corresponding to the red-framed region in (b–d), showing the nucleation and climb of GB dislocations during the grain rotation.

also induce a torque (e.g., clockwise) that leads to the grain rotation, as seen in Supplementary Fig. 2 (also see Fig. 34 in reference 29). According to Cahn's prediction [30], the relation between the grain rotation angle and migration distance is $dr = -r\frac{d\theta}{\beta}$ (here, r is the grain size, β is the coupling coefficient, θ is the misorientation angle between the two adjacent grains). This disconnection mechanism is assisted by local atomic shuffling and short-range atomic diffusion, which are likely to occur at low temperatures.

Interestingly, in addition to GB migration, there are other important GB activities going on at the GB_{1-4} as well. Specifically, the generation, glide and climb of GB dislocations appear to have also occurred at the mixed GB, reminiscent of the inter-grain dislocation activities depicted by Frank and Bilby [23,24] and Li et al. [21]. As the first indication of this, let us take another look at the magnified HRTEM images in Fig. 3e–g, which correspond to the red boxed region in Fig. 3b–d, respectively. As indicated by the red dashed lines in Fig. 3e, the edge-on (111) planes in G_1 smoothly switch to the edge-on (100) planes in G_4, and a dislocation (labeled as "1″) is observed at GB_{1-4}; this inter-grain dislocation is readily identified by an extra half (010) plane in G_4. During subsequent grain rotation, Fig. 3f shows that a new inter-grain dislocation (labeled as "2″) is formed, and the local interface structures of GB_{1-4} become very sharp. Since most of the grains have sizes less than ~ 10 nm, we believe that most of these dislocations should be nucleated from the GB, as previous MD simulations and experiments results indicate that the GBs serve as sources of dislocations in NC metals [19,46,47]. Comparison of the positions of dislocation "1″ and dislocation "2″ in Fig. 3f and Fig. 3g suggests that these dislocations have climbed along GB_{1-4}. The dislocation climb is realized through short-range diffusion at relatively low temperature. In other words, beside the disconnection model, the Frank–Bilby dislocations resulted grain rotation [23,24] appears to also play a significant role. Taken together, Figs. 2 and 3 above demonstrate that the grain rotation at the general GBs is actually accomplished via GB dislocations in combination with atoms shuffling and disconnection activities. In other words, a combination of disconnection and Frank–Bilby dislocations, with assistance of local shuffling of atoms, are required to explain the grain rotation with GB migration at mixed GBs.

Our in situ atomic-scale observations show that the GB dislocation density at GB_{1-4} has changed a lot, based on a comparison of the images before and after the grain rotation (Supplementary Fig. 3). The generation/removal of GB dislocations changes the total number of dislocations at the GB, and the dislocations adjust their distance with each other via climb and glide in the GB. This process increases/decreases the density of dislocations at GB (changing the average distance between dislocations), thus leading to the grain rotation. To gain an in-depth understanding of the GB dislocation nucleation and motion in GB plane, we zoom into the yellow-boxed region in Fig. 4a, and use the magnified HRTEM images in Fig. 4b–h to track the profuse activities of the inter-grain dislocation at GB_{1-4} (this is in a same region from that in Fig. 3a-d).

The first atomic layer at the bottom of G_1 is taken as a reference (marked by a yellow solid line). Relative to this first layer, all the adjacent atomic layers are numbered to facilitate the tracking of the inter-grain dislocation movement during grain rotation. In the current study, the atomic layer at the bottom of G_1 is taken as a reference (labeled as 1), and from Fig. 4b–h, one can observe that the contrast of the HRTEM images and the first atomic layer has not changed, which indicates that there is no significant change in defocus or height during this loading process. In addition, the defocus change can lead to the contrast of HRTEM images change, but it cannot lead to a change in position of these GB dislocations (as can be found in the HRTEM simulation from Supplementary Fig. 4). Thus, confirming that the observed dislocation motion at the GB should result from straining. Fig. 4b shows two types of inter-grain dislocations at GB_{1-4}, as marked by the yellow

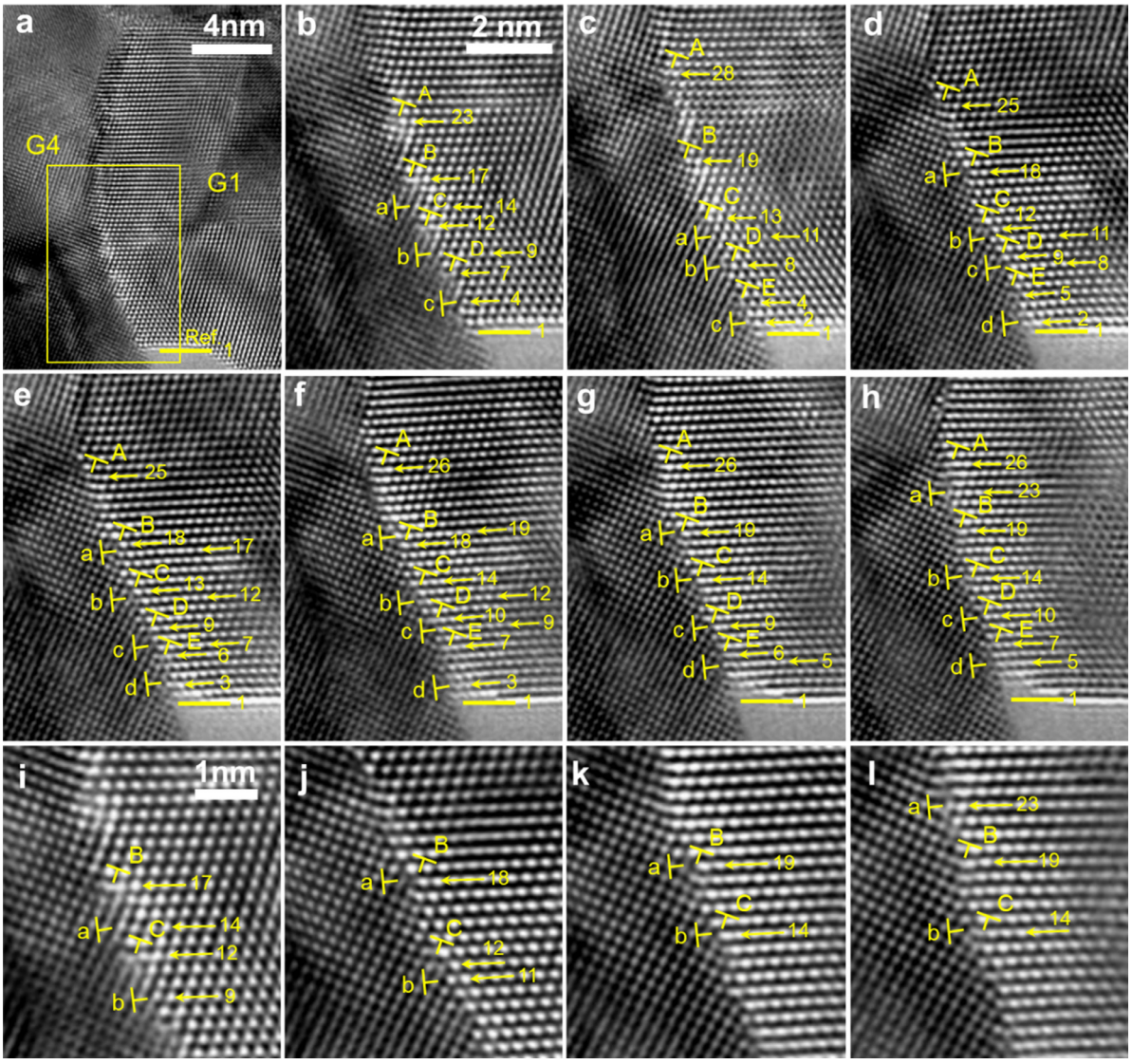

Fig. 4. In situ observation of the generation, climb, and interaction of GB dislocations at GB_{1-4} during grain rotation. (a) An HRTEM image at the early stage of grain rotation. (b–h) A series of enlarged HRTEM images of the yellow boxed region in (a). In (b), the lattices between G_1 and G_4 have a nearly perfect match; two types of dislocations (marked by yellow "T") are observed in GB_{1-4}. One type of dislocations, labeled as "A, B, C, D" are located at the 23rd, 17th, 12th, and 7th atomic layers, respectively, while another type of dislocations labeled as "a, b, c" are located at the 14th, 9th, and 4th atomic layers, respectively. In (c), a new GB dislocation "E" nucleates, and the GB dislocations also climb. As shown in (d–h), the rotation between G_1 and G_4 leads to the nucleation of a new GB dislocation, the climb of GB dislocations, and the reaction product of a Lomer-like dislocation at the GB. (i–l) Enlarged HRTEM images (corresponding to (b), (d), (g), and (h) to focus on the atomic-scale process of climb of GB dislocations B, C and a, b.

"T". One type of inter-grain dislocation features an extra half (010) plane in G_4 and these dislocations are labeled by capital letters, such as "A, B, C and D". The cores of these GB dislocations are located at the 23rd, 17th, 12th, and 7th atomic layers, respectively. Another type of inter-grain dislocation features an extra half (111) plane in G_1 and these dislocations are labeled by lowercase letters, such as "a, b and c". The cores of these dislocations are located at the 14th, 9th, and 4th atomic layers, respectively. During the grain rotation, as shown in Fig. 4c, a new inter-grain dislocation E nucleates. Meanwhile, dislocations "A", B, C, and D climb up, as their cores move to the 28th, 19th, 13th, and 8th atomic layers, respectively, whereas dislocations "a", b, and c glide along the GB plane, with their cores moving to the 11th, 8th, and 2nd atomic layers, respectively. It should be noted that this is different from the traditional lattice dislocation slip (glide on {111} planes towards the interior of the G_1). As shown in Fig. 4d, continued grain rotation between G_1 and G_4 leads to the nucleation of a new inter-grain dislocation d. At the same time, dislocations a, b, and "c" glide up to the 18th, 11th, and 8th atomic layers, respectively, whereas dislocations A, B, and "C" climb down to the 25th, 18th, and 12th atomic layers, respectively, and dislocations D, and E climb up to the 9th and 5th atomic layers, respectively.

Interestingly, dislocation a glides to react with dislocation "B" and forms a Lomer-lock-like structure at the GB. The subsequent process of GB dislocation climb shown in Fig. 4e–h is similar to that in Fig. 4b–d. The structure of these GB dislocation locks is very like the Lomer locks that generated by lattice dislocation reaction in fcc lattice with Burgers vector of $\frac{1}{2}$<110> type. While it should be taken care that the Burgers vector at mixed GB is different from that in lattice, thus, the core structure of this Lomer-lock-like structure at the GB is different from that in lattice (see Supplementary Fig. 5). Interestingly, these Lomer-like dislocations dissociate with further grain rotation (Fig. 4e, 4f), such that the climbing and gliding of GB dislocations meet with each other to

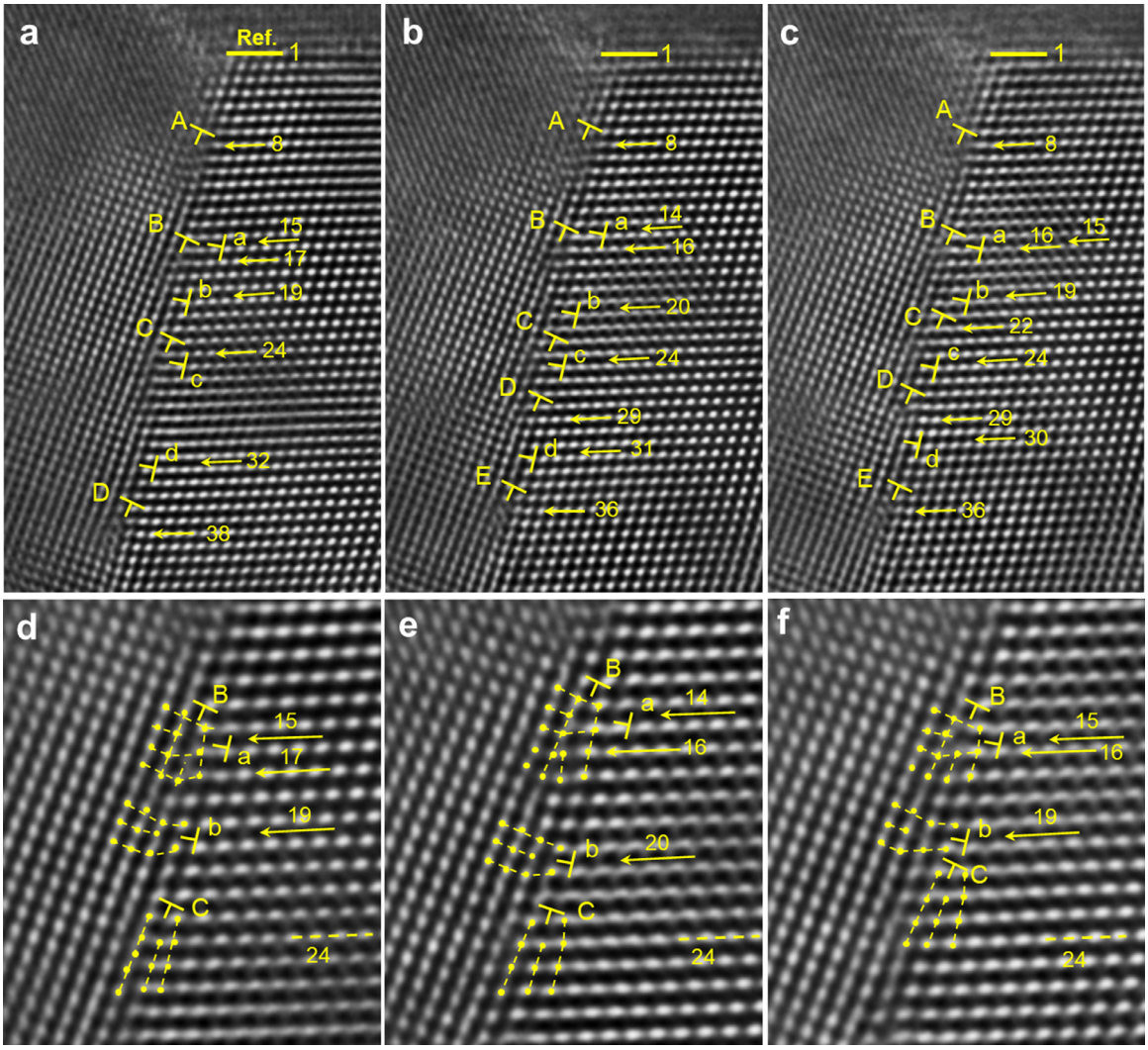

Fig. 5. In situ observation of the atomic-scale processes in the upper part of GB_{1-4} during grain rotation. The local GB structures are different from those in Fig. 4, as a different GB plane is involved here. (a) Two types of dislocations (marked by yellow "T") are observed in GB_{1-4}, and they are labeled as "A, B, C, D" and "a, b, c, d", respectively. The locations of the cores of these dislocation positions are indicated by the number of atomic layers as defined in Fig. 4. (b, c) During the grain rotation, the two types of GB dislocations climb up and down, respectively. (d, e) Enlarged HRTEM images zooming into the climb-up and climb-down processes of GB dislocations "B, C" and "a, b". The core structures of these dislocations are highlighted by yellow lines and dots. (f) Dislocation "B" climbs up by one atomic layer to meet dislocation a, forming a Lomer-lock-like structure at the GB.

form new Lomer-like dislocations at GB_{1-4} (Fig. 4g, 4h). Fig. 4i–l present enlarged HRTEM images (corresponding to Fig. 4b, d, g, and h, respectively) that clearly show the climb of GB dislocations B, C and a, b. Specifically, in Fig. 4i, dislocations B, C and a, b locate at different atomic layers; in Fig. 4j, dislocation B climbs up by one atomic layer and dislocation a glides up by four atomic layers; as a result, these two dislocations meet with each other (at the 18th atomic layer) to form a Lomer-like dislocation [35]. In Fig. 4k and 4l, two Lomer-lock-like structures are formed and then unlocked as the inter-grain dislocations climb and glide. Previously, the Lomer structure was believed to be formed by the reaction of intra-grain gliding dislocations inside large grains [35]. The inter-grain dislocation climb, glide, and reaction observed here are interesting and have never been reported.

Fig. 5 illustrates the action in another section of GB_{1-4}, involving a different GB plane: there are several steps on GB segment that appear quite different from those in Fig. 4. Our objective is to examine if this change in GB structure alters the mechanism. Here again the formation and destruction of GB Lomer-lock-like structures are frequently observed. In this case, the 1st atomic layer on the upper part of G_1 is taken as the reference (marked by a yellow solid line). In Fig. 5a, two types of GB dislocations are marked using yellow "T". One type features an extra half (010) plane in the lattice of G_4, labeled as "A, B, C, D, …", with the respective dislocation cores at the 8th, 17th, 24th, and 38th atomic layers (indicated by yellow arrows). Another type features an extra half (100) plane in the lattice of G_4, labeled as "a, b, c, d, …", with cores at the 15th, 19th, 24th, and 32nd atomic layers (indicated by yellow arrows). During the grain rotation, Fig. 5b, a new GB dislocation "E" nucleates at the 36th layer, without appreciable movement of dislocations A and c. Meanwhile, dislocations B, D climb up to the 16th and 29th atomic layers, and dislocations a, b, d glided to the 14th, 20th, and 31st atomic layers, respectively. Upon continued grain rotation, Fig. 5c, dislocation "C" climbs up to the 22nd atomic layer, and b glides up to the 19th atomic layer again. Enlarged HRTEM images in Fig. 5d–f clearly show the climb and glide of GB dislocations B, C and "a, b", with their core structures highlighted by yellow dot-dash lines. Fig. 5d and e show that dislocation "B" and b move up and down respectively, while dislocation a glides up by one atomic layer and dislocation C does not move.

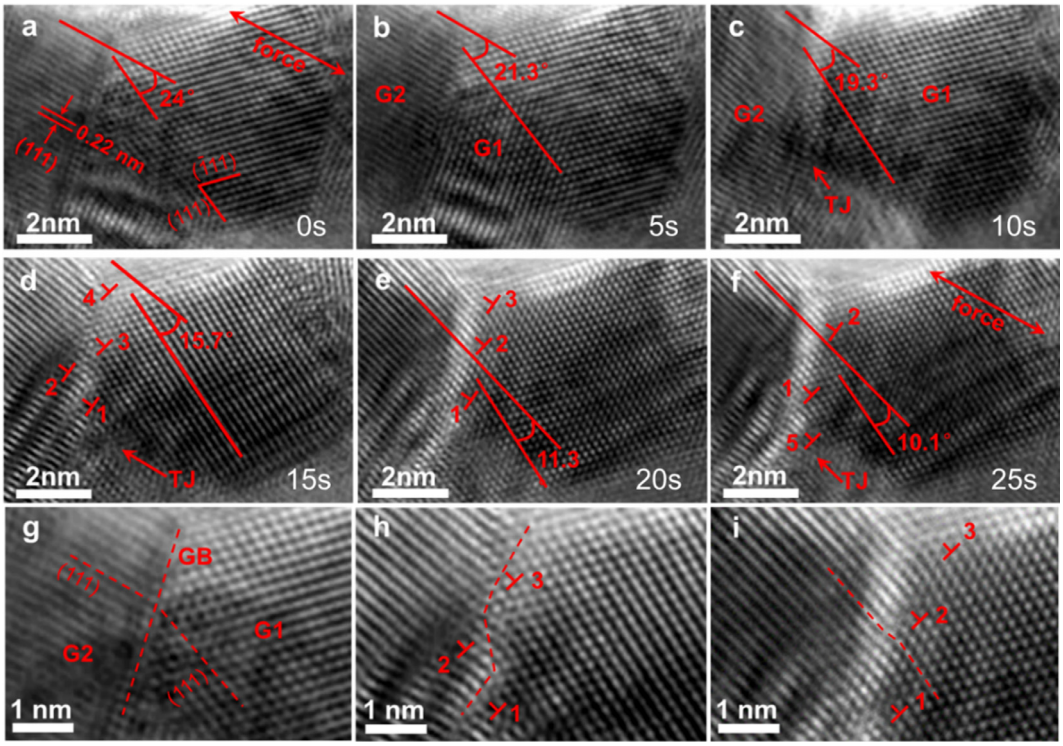

Fig. 6. Another example of rotation of a ~7 nm-sized grain. (a) The grain G_1 exhibits a clear [01$\bar{1}$] axial lattice, while the grain G_2 exhibits fringes, indicating that GB_{1-2} is a mixed GB. (b, c) During straining, grain rotation occurred between G_1 and G_2, leading to a decrease in the misorientation angle across GB_{1-2} from 24° to 19.3° (d–f) With further straining, a high density of GB dislocations at GB_{1-2} was observed, along with climb of GB dislocations (marked by "T"); the number of dislocations at GB_{1-2} decreased, leading to a decrease in the misorientation angle across GB_{1-2} from 15.7° to 10.1° (g–i) Enlarged HRTEM images corresponding to (a, d, e), respectively.

As seen from Fig. 5f, dislocation "B" climbs up by one atomic layer, and it combines with dislocation a to form a Lomer-lock-like structure. All these observations (Figs. 4 and 5) indicate that what we are seeing is a universal and inevitable path through which the climbing and gliding GB dislocations interact.

Lomer locks are well known dislocation locks that are usually generated via two full dislocations mutually knit with each other in the lattice. Because these Lomer locks are in neither of the initial glide planes (i.e., the closely packed {111} planes), they are an obstacle to other dislocation gliding in lattice [35,48]. In the current study the Lomer-lock-like structures were at the GB, the nature of this dislocation and the corresponding activities are different from those in the lattice. These Lomer-lock-like structures at the GB do not slip on the close packed {111} planes of the lattice, but glide and climb along the GB. The highly distorted lattice at the GB and the relatively large excess volume (see the pentagonal core structure in Fig. 5d–f) can widen the diffusion channel, and thus, will promote the GB dislocation climb. Previous studies show that during the deformation, the diffusion will occur in the region with large excess volume at the GB [49–51]. Many studies also show that the mass transport rate at the triple-junction of the GB is relatively higher than that of the GB, indicating that the large excess volume promotes the diffusion [51–53]. Thus, we believe that the Lomer-like dislocations at the GB do not impede the dislocation motion; by contrast, they widen the diffusion channel that promotes the grain rotation.

To demonstrate the general applicability of the combination of the Frank–Bilby dislocation activities with atomic shuffling and disconnection activities for the mixed GBs revealed in Fig. 3-5, Fig. 6 shows the rotation of a ~7 nm-sized grain with another type of mixed GBs, in which one grain exhibits the [01$\bar{1}$] axial lattice whereas another only exhibits lattice fringes. Our in-situ observation shows that the aforementioned rotation mechanism is also valid for this type of grain. As can be observed from Fig. 6a, G_1 exhibits a clear [01$\bar{1}$] axial lattice; however, G_2 is not closely aligned with a crystallographic direction, and thus exhibits some lattice fringes. The angle between the edge-on (111) plane in G_1 and the edge-on (111) plane in G_2 is ~24° We can see that the interface between the adjoining grains G_1 and G_2 is relatively sharp. During grain rotation, the edge-on (111) planes in G_1 smoothly over a few planes to the edge-on (111) planes in G_2, as observed in Fig. 6b–c, which are similar to those observed in Fig. 3. Meanwhile, the shape of GB_{1-2} changed slightly, indicating that GB migration occurred via more local shuffling and/or short-range atomic diffusion. Thus, we believe that this grain rotation should also be governed by the nucleation and motion of disconnections [29,30] assisted by local atomic shuffling and short-range atomic diffusion. Based on the classical theoretical model, the grain rotation coupled with GB migration should be governed by the disconnection motion that glide along the GB plane. The glide of disconnection induces a torque that leads to the grain rotation, and this could lead to a stepwise structure on the GB [54-57]. Such steps on the GBs are hallmark feature of the disconnection gliding [29,58]. In current study, many steps were observed on the GBs (Fig. 2d-g and Supplementary Fig. 6), which further confirmed the disconnection activities involved during the grain rotation process. These disconnection glide along the GB that led to the GB migration accompanying the grain rotation (also see the schematic view illustrated in Supplementary Fig. 2). With further straining, a high density of GB dislocations was observed at GB_{1-2} (Fig. 6d). Fig. 6d–f show that the number of GB dislocations at GB_{1-2} decreased, and their average spacing increased from 1.01 to 1.71 nm, causing a decrease in the misorientation angle across GB_{1-2} from 15.7° to 10.1° Fig. 6g–i present enlarged HRTEM images that correspond to Fig. 6a, d, and e, respectively. As indicated by the red dotted lines in Fig. 6g, the interface between G_1 and G_2 was atomically sharp, and the edge-on

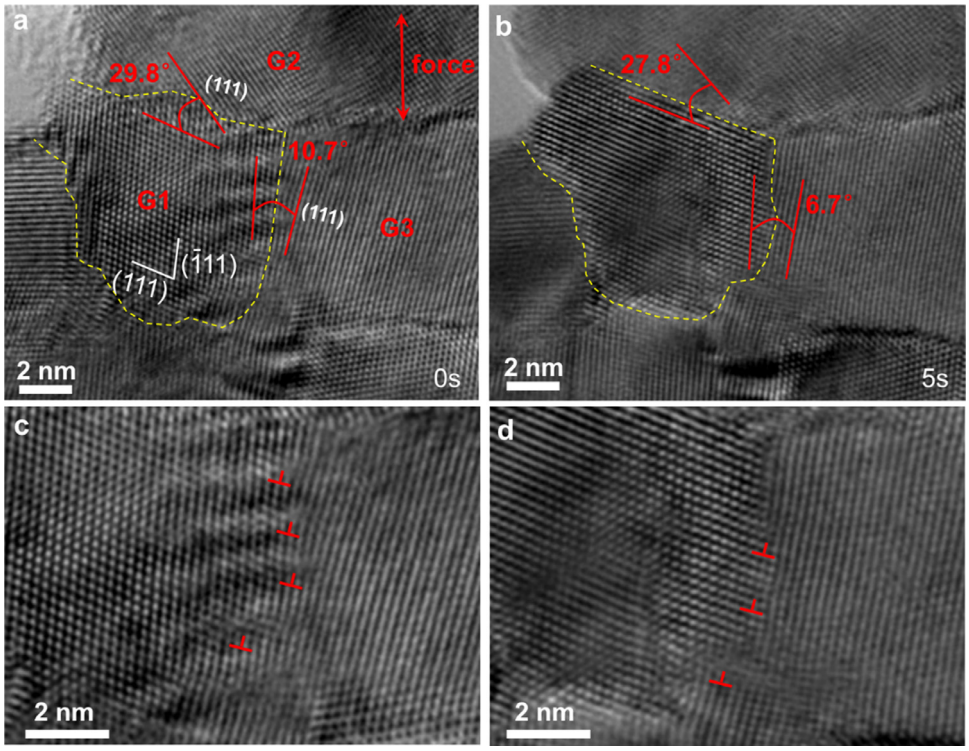

Fig. 7. An example illustrates the atomic-scale grain rotation process of a ~ 7 nm-sized grain. (a) The G_1 exhibits a clear [01$\bar{1}$] axial lattice, where the {111} lattice/plane is noted, while G_3 exhibits fringes, indicating the GB_{1-3} is a mixed GB. The angles between the edge-on {111} plane in G_1 and the edge-on {111} plane in G_2 and G_3 are ~29.8° and 10.7°, respectively. (b) During the grain rotation, as noted by "*T*," the number of dislocations at GB_{1-3} decreases, leading to a decrease in the misorientation angle of GB_{1-3} from 10.7° to 6.7° Meanwhile, the misorientation angle of GB_{1-2} changed from 29.8° to 27.8° Additionally, the GB structure and the morphology of GB_{1-2} and GB_{1-3} have changed substantially (as the yellow line notes), indicating GB migration is an important accommodation mechanism of grain rotation for those mixed GBs. (c, d) Enlarged HRTEM images which are corresponding to (a), (b) give a better visualization of the decrease in dislocations at GB_{1-3}.

(111) planes in G_1 did not continuously switch to the edge-on (111) planes in G_2. As indicated by the red dotted lines in Fig. 6h and i, both the position and structure of GB_{1-2} changed markedly, and the edge-on (111) planes near GB_{1-2} were continually strained, similar to the corresponding cases in Figs. 4 and 5. During in-situ straining, G_1 and G_2 exhibited no appreciable changes in their lattice fringes, indicating that grain rotation was not caused by the tilt deformation of grains in the specimen. During the straining, G_1 and G_2 exhibited no obvious change in the lattice fringes, indicating that the grain rotation is not caused by a global tilt of the specimen during deformation. Otherwise, the lattice or fringes would go out of contrast as the diffracting planes are rotated away from the beam.

It is noted that grain rotation is actually a collective rotation process of the surrounding grains, i.e., the surrounding grains also participate in rotations relative to one another in a coordinated manner. Fig. 7 shows a typical example of several grains rotating in a coordinated manner. As can be observed from Fig. 7a, G_1 exhibits a clear [01$\bar{1}$] axial lattice, whereas G_2 and G_3 exhibit fringes, indicating that GB_{1-2} and GB_{1-3} are mixed GBs. The angles between the edge-on {111} plane in G_1 and the edge-on {111} plane in G_2 and G_3 are ~29.8° and 10.7°, respectively. During the grain rotation, as noted by "*T*," the number of dislocations at GB_{1-3} decreased, leading to a decrease in the misorientation angle of GB_{1-3} from 10.7° to 6.7°, as shown in Fig. 7b. Meanwhile, the misorientation angle of GB_{1-2} changed from 29.8° to 27.8°, as shown in Fig. 7b. Additionally, the GB structure and the morphology of GB_{1-2} and GB_{1-3} changed substantially (as shown by the yellow line), indicating that GB migration was an important accommodation mechanism of grain rotation for those mixed GBs. The surrounding grains also underwent GB migration and rotation process during straining; this proves that the surrounding grains rotate collectively in a coordinated manner. Fig. 7c and 7d exhibit enlarged HRTEM images corresponding to those in Fig. 7a and 7b, which show the decrease in dislocations at G_{1-3} more clearly. This grain rotation accompanied with GB migration indicated that the surrounding grains also rotate collectively via combined GB dislocation activities, as well as atomic shuffling and disconnection activities. We performed in situ observations of more than 20 GBs. The statistical results of rotation angle versus GB migration distance for mixed GBs are shown in Fig. 12. For these mixed GBs (yellow dots), their rotation occurs through a combination of the Frank–Bilby dislocation activities with atomic shuffling and disconnection activities, leading to significant GB migration. Further, the GB migration distance increases with rotation angle.

We also investigated the atomic-scale mechanisms of grain rotation associated with tilt GBs. During grain rotation, the atomic-scale deformation of these tilt GBs can be reasonably characterized by the Frank–Bilby dislocation activities, while GB migration is not as obvious as that observed for mixed GBs. Fig. 8a–c display three HRTEM images showing the atomic-scale grain rotation process that involved a tilt GB. As shown in Fig. 8a, both G_1 and G_2 exhibit a clear [110] axial lattice, indicating that GB_{1-2} is a tilt GB. From Fig. 8a, the measured GB angle for GB_{1-2} is ~22.1°, indicating that GB_{1-2} is obviously a high-angle GB, while this GB can also roughly serve as a dislocation GB that has a high density of Frank–Bilby dislocations [59]. Comparing the GB structure in Fig. 8a–c, G_1 and G_2 underwent a rotation process, and the number of dislocations at the GB decreased. As revealed in Fig. 8c, the number of dislocations at the GB decreased, which led to a decrease in the misorientation angle of GB_{1-2} from 22.1° to 14.7° This process occurs via glide and climb of the GB Frank–Bilby dislocation, and it

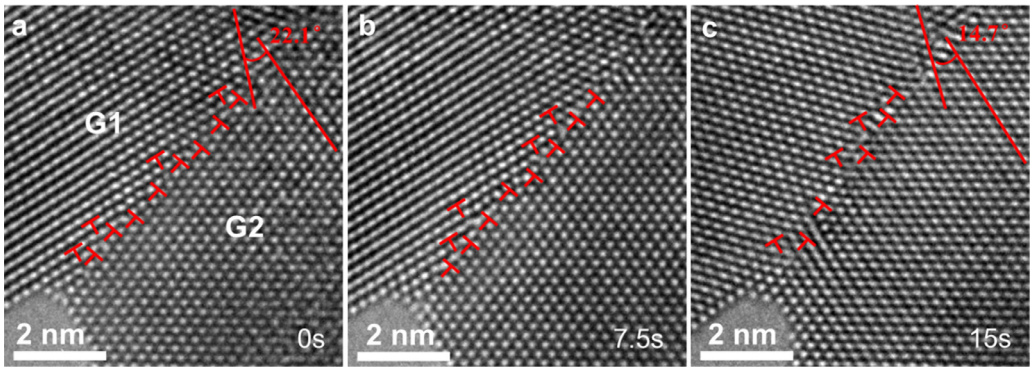

Fig. 8. An example shows the grain rotation process of a tilt GB and both the G_1 and G_2 exhibit a clear [110] axial lattice. (a–c) During the straining, G_1 and G_2 undergoes a rotation process, leading to a decrease in the misorientation angle of G_{1-2} from 22.1° to 14.7°, and high density of GB dislocations at GB_{1-2} are observed, as noted by "T".

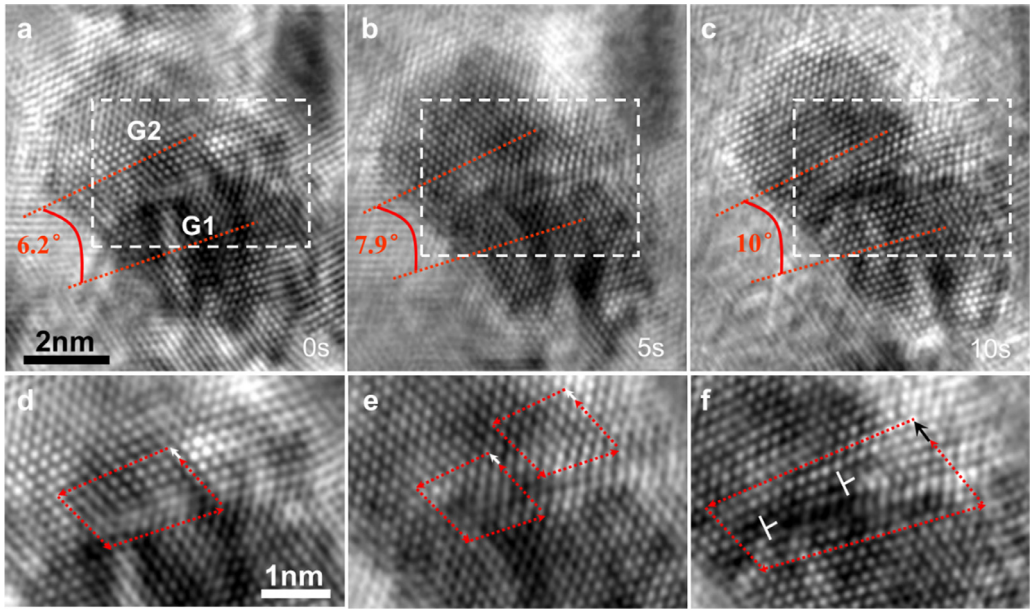

Fig. 9. Another example shows the atomic-scale grain rotation process of a tilt GB. (a) Both the G_1 and G_2 exhibit a clear [110] axial lattice, indicating the GB_{1-2} is a tilt GB. (b, c) During the grain rotation, as noted by "T" the number of dislocations at GB_{1-2} increases, leading to an increase in the misorientation angle of GB_{1-2} from 6.2° to 10° (d-f) Enlarged HRTEM images which are corresponding to (a-c) show the increase in dislocations at GB_{1-2} more clearly.

is similar to that shown in Fig. 4 and Fig. 5 and with neglected GB migration. The rotation of G_1 and G_2 leads to the original high-angle GB being transformed into a low-angle GB. After the GB_{1-2} is transformed into a low-angle GB, the rotation model follows the nucleation and climb of GB dislocations. The difference is mostly the tilt GB's rotation via Frank–Bilby dislocation activities with neglected GB migration, which is different from that shown in several previous postmortem TEM results [29,31,60].

To demonstrate the general applicability of the Frank–Bilby dislocation activities that resulted in rotation for the tilt GBs, Fig. 9 shows another example of rotation of a ~7 nm-sized grain, which also involved a tilt GB. As can be observed from Fig. 9a, both G_1 and G_2 exhibit a [110] lattice, indicating that GB_{1-2} is a tilt GB, and the measured GB angle for GB_{1-2} is ~6.2° As shown in Fig. 9, the tilt GBs naturally contain GB dislocations [29]. As indicated in Fig. 9a–c, during the straining, the number of dislocations at GB_{1-2} increases and leads to an increase in the misorientation angle of G_{1-2} from 6.2° to ~10° Fig. 9d–f provide enlarged HRTEM images corresponding to Fig. 9a–c, which show the increase in dislocations at GB_{1-2} more clearly. It can be observed that the grains separated by tilt GBs rotated with less GB migration. In the current experiments, there is no obvious trend suggesting that the GB migration distance increases with rotation angle, which is different from the observation for the grains separated by mixed GBs. Such tilt GBs naturally contain a high density of Frank–Bilby dislocations [29] and can thus rotate without obvious GB migration, which is in contrast to the corresponding results at mixed GBs. We also examined many other grains with tilt GBs, and our results show that for the grains surrounded by tilt GBs, most of them rotate via the generation/annihilation, glide, and climb of the Frank–Bilby dislocation, with no obvious GB migration (also see MD simulation in Fig. 10). GB migration is far less obvious than that observed for mixed GBs. In other words, the rotation of grains surrounded by tilt GBs always conform to the Frank–Bilby dislocations [20–23,61,62]. Many previous studies suggested that the grain rotation occurred with neglected GB migration; however, many other reports suggested that grain rotation was always coupled with GB migration [3,7,17,19,20,35,61–65]. Our results show that whether the grain rotation is coupled with GB migration or not depends on the type of GBs. The previous reports on grain rotation both with and without GB migration could be the result of studies dealing with different types of GBs.

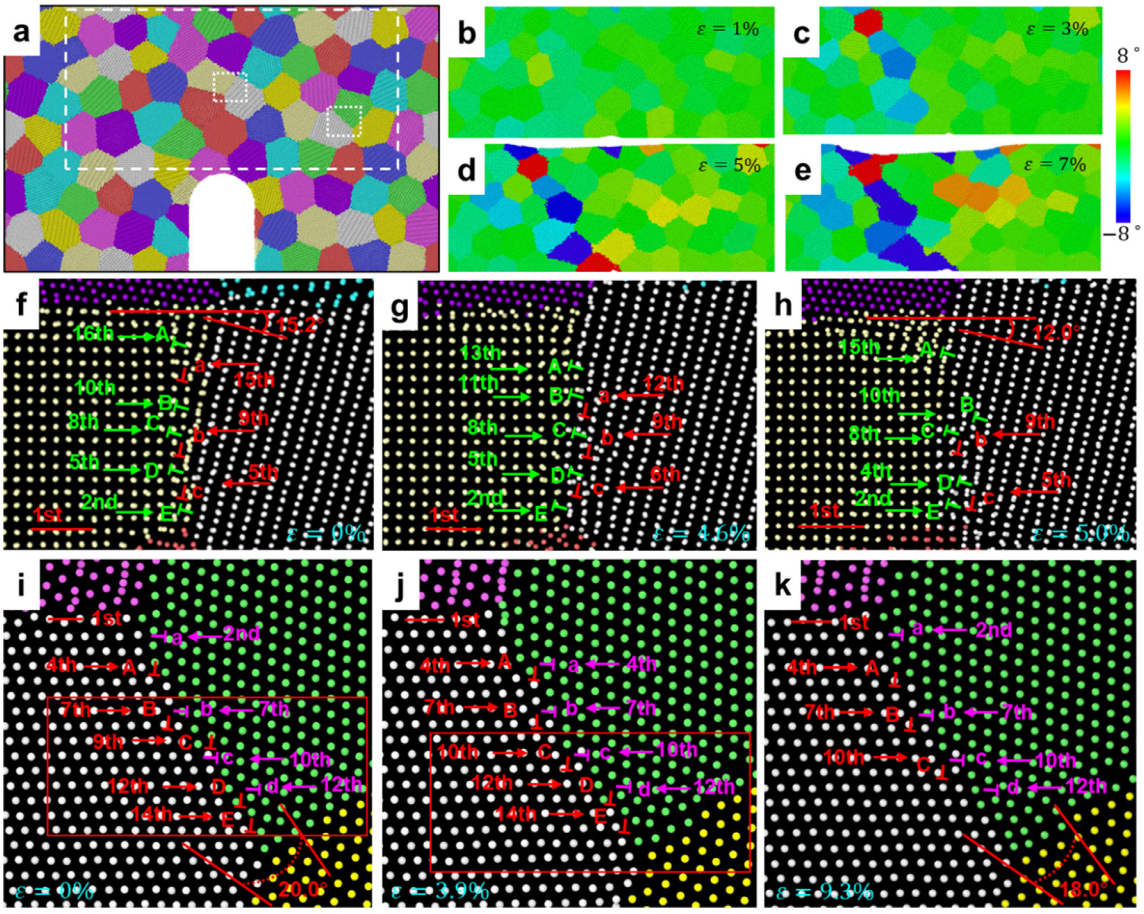

Fig. 10. Molecular dynamics simulation results showing atomic mechanisms mediating grain rotation. (a) Polycrystalline Pt thin film model constructed for the MD simulation. (b–e) Different colors showing the change in misorientation angle to monitor the grain rotation, at strain of 1%, 3%, 5% and 7%, respectively. (f–h) A typical example of grain rotation for grains separated by a mixed GB, both the GB migration and inter-grain dislocation activities are observed, indicating that the grain rotation about mixed GBs proceeds via the Frank–Bilby dislocation activities together with atomic shuffling and disconnection activities. (i–k) A typical example of grain rotation for grains separated by a tilt GB. The grain rotation in this case is mediated by inter-grain dislocations activities with no obvious GB migration. The inter-grain dislocations activities lead to the frequent formation and destruction of Lomer-lock-like structure at both the mixed and tilt GBs.

3.3. Atomistic mechanisms of mixed and tilt grain boundaries during grain rotation in MD simulation

MD simulations lend further credence to the observed mechanisms of grain rotation and their dependence on the type of GBs involved. To compare with experiments, we constructed a model of polycrystalline Pt with length, width, and thickness equal to 65, 40, and 8 nm, respectively (Fig. 10a). The average grain size in the thin slab is ∼ 6 nm. A U-shaped edge notch is created with a tip radius of 5 nm and a length of 15 nm [26]. Tracking the movement of the atoms in the center of each grain, the rotation angle of the grains can be directly measured. Fig. 10b-e show the grain rotation angle upon straining the model to 1%, 3%, 5% and 7%, respectively. The color variation from red to blue indicates the grain rotation angle values from 8° to −8° Obviously, many gains undergo the rotation process. Fig. 10f-h show a typical example of grain rotation for grains separated by mixed GB, the corresponding strains were 0%, 4.6%, 5.0%, respectively. The rotation angle between the two grains in this figure is ∼ 3.2°, and the GBs positions have obviously moved. In other words, GB migration accompanies the rotation. In the meantime, GB dislocation activities are abundant. As noted in Fig. 10f, two types of inter-grain dislocations are present at the GB, as marked by red and green “T”, one type labeled “A, B, C, D, E”, and the other type “a, b, c”. Before the deformation, dislocations “C” and b combine to form a Lomer-lock-like structure. During grain rotation, Fig. 10g, dislocations A, B, a, c undergo the climbing and gliding process, during which “B” interacts with a, and D with c, to form two Lomer-lock-like structures. As shown in Fig. 10h, the continued grain rotation leads to the annihilation of dislocation “a” and that resulted in the destruction of a Lomer-lock-like structure. At the same time, dislocations A, B, D, c undergo the climbing and gliding process. All these corroborate what we have observed for mix boundaries in the TEM experiments. In current MD simulations, we adopt a stepwise loading [25,26,39,44], such that the lowered strain rate gives enough time for short-range diffusion or shuffling that lead to dislocation climb (see method section for more details). The dislocation climb is realized through short-range diffusion, in which these atoms near the dislocation core only travel very short displacement (less than 2 Å). Theses make the dislocation climbing in the interface/GB to occur on MD time scale even at room temperature. This kind of short-range atomic diffusion (Fig. 1-3, and Fig. 7 in reference 67) and dislocation climb were also observed in previous MD simulation in NC metals [66,67].

With regards to tilt GBs, MD simulations also reinforce the notion that grain rotation can be completed with the Frank–Bilby dislocation activities, consistent with the TEM observations (As shown in Fig. 8 and 9). Fig. 10i–k provide three snapshots that show a typical example of grain rotation for two grains separated by a tilt GB; the corresponding strains are 0%, 3.9%, 9.3%, respectively. The rotation angle between these two grains (the grains with white atoms and green atoms) was ∼ 2°, while there is no obviously GB

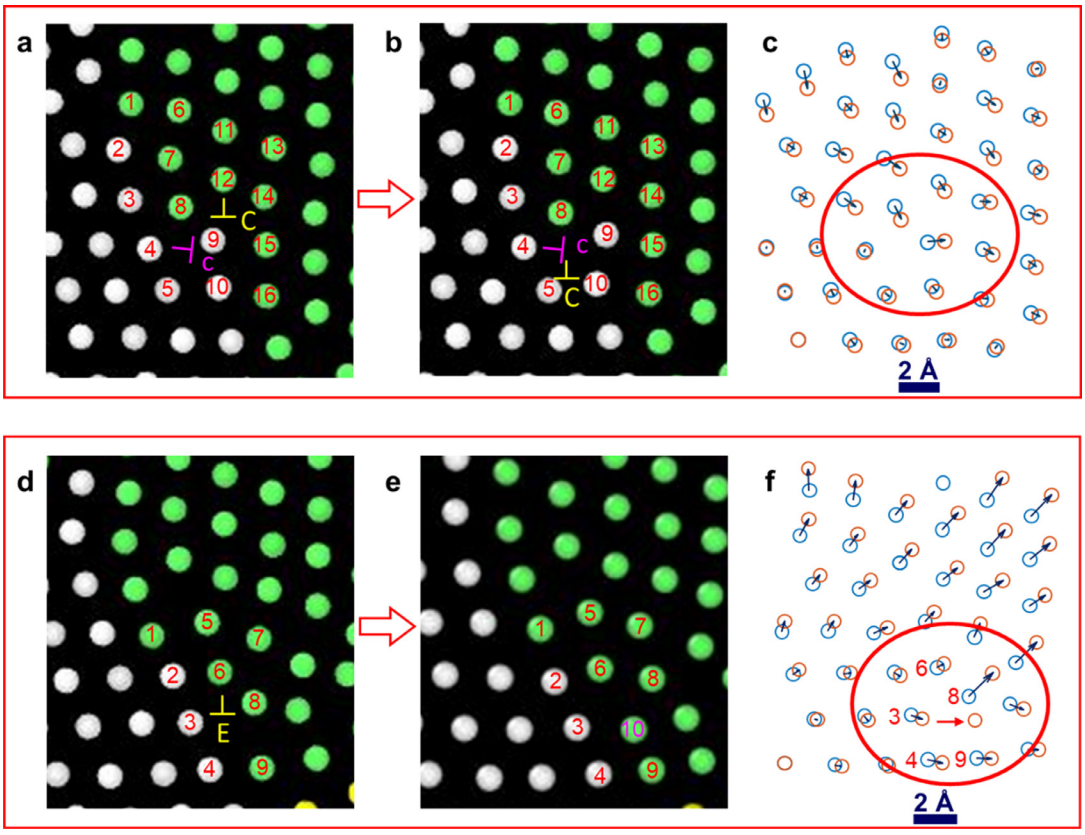

Fig. 11. The short-range diffusion of atom-columns at GB. (a) The enlarged MD image corresponding to the red framed region in Fig. 10i showing the two separated dislocation "C, c". (b) The enlarged MD image revealing these two dislocations reaction with each other to form a Lomer-like dislocation. (c) The displacement map extracted by automated analysis. Atom-columns at different strain are represented by different colors. Each segment represents the displacement vector of an atom column between two consecutive images in (a, b), and the length of each segment represents the magnitude of the displacement. (d) The enlarged MD image from the red framed region in Fig. 10j showing the dislocation "E". (e) The enlarged MD image showing this dislocation climbing toward the triple junction. (f) The displacement map extracted from (d, e), and the red arrow indicates the atom-columns '10′ diffused to the core of dislocation E. .

migration observed by comparing the GBs positions in Fig. 10i–k. As shown in Fig. 10i, the GB angle between these two grains (the grains with white atoms and green atoms) is ~ 20° Since the grains in the simulation model are very small, the entire GB can be composed of inter-grain dislocations [21], as marked by red and pink "T". We can identify two Lomer-like dislocations at the GB. During the grain rotation, as shown in Fig. 10j, dislocations a, C undergo the climbing and gliding process, and this leads to the interaction of a with A to form another Lomer-like dislocations. In Fig. 10k, further grain rotation is mediated by the gliding process of "a", accompanied by the annihilation of D and E. As a result, only two Lomer-lock-like structures are left.

Our MD simulation also provides a deep insight into the atomic-scale dislocation motion along the GB, which reveals that this process only needs short-range diffusion of atom-columns at the GB. Fig. 11a shows an enlarged image presents two separated dislocations labeled as "C" and c at this GB (corresponds to Fig. 10i), where the core of dislocation C is located at the atom-column '12' and the core of dislocation c is located at the atom-column '4'. During the grain rotation, as exhibited in Fig. 11b (corresponds to Fig. 10j), the atom-columns near these two dislocations underwent short-range diffusion, where atom-column '9′ moved toward the up-right side and other atoms moved accordingly, and therefore, these two dislocations moved and reacted with each other to form a Lomer-like dislocation. Fig. 11c shows the displacement map of these atom-columns. Comparing the Fig. 11a and 11b with the previous method, it can be observed that these atom-columns near the dislocation core only have a very short displacement, of less than 2 Å. In addition to the short-range diffusion resulting from GB dislocation motion and reaction, the MD simulation also revealed that the triple junction is an important source and sink of GB dislocation. Fig. 11d shows an enlarged image that presents a dislocation labeled as "E" at this GB (corresponds to Fig. 10j), where the core of dislocation E is located at the atom-column '6'. During grain rotation, an atom-column (labeled as '10') that from triple junction diffused to the core of dislocation E, and the dislocation climbed toward the triple junction (corresponds to Fig. 10k). This type of short-range atomic diffusion (Fig. 1-3, and Fig. 7 in reference 67) and dislocation climb was also observed in previous MD simulations in NC metals [66,67]. The above results revealed that the atoms near the dislocation core only travel a very short distance, and hence the dislocation climbing\gliding that resulted in grain rotation occur easily, even at room temperature. These results of our experiments provide clear atomistic mechanisms of the motion and generation\annihilation of GB dislocation.

In Fig. 12, we plot the grain rotation angle vs GB migration distance, for the mixed and tilt GB. The data from both experiments and MD simulations are included. For the mixed GBs (yellow dots), their rotation occurs through a combination of the Frank–Bilby dislocation activities together with atomic shuffling and disconnection with significant GB migration, and the GB migration distance increases with rotation angle. In contrast, for the tilt GBs (the purple triangles in Fig. 12), the rotation can be accounted for by the generation, climb, glide and reaction of GB dislocations, with no obvious scaling of the GB migration distance with the rotation angle. The GB migration distances are mostly very small, below ~ 0.9 nm. Thus, our in situ atomic-scale direct observation and MD simula-

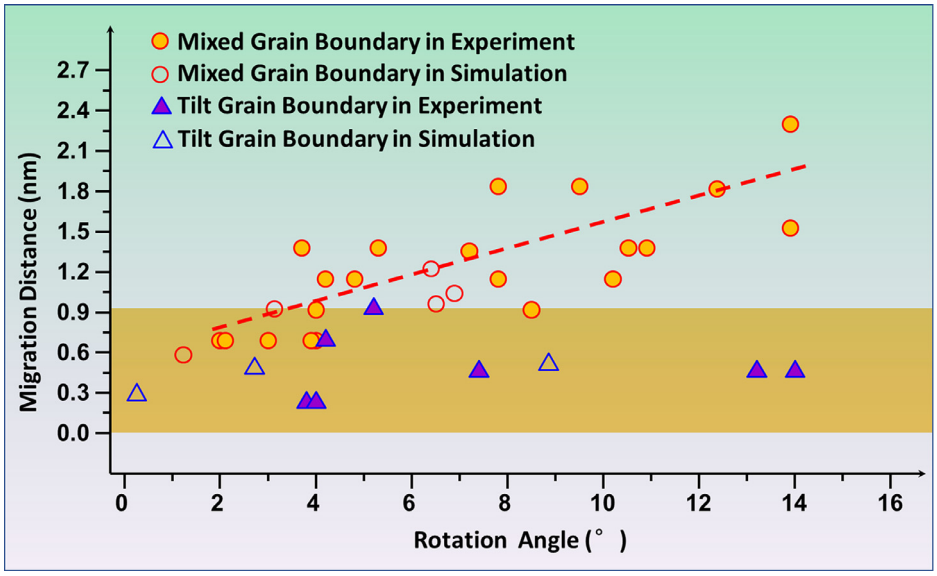

Fig. 12. Grain rotation angle vs GB migration distance for the mixed and tilt GBs **with two grains belong to [110] axial lattice**. The yellow dots show that the migration distance of mixed GBs increases with increasing rotation angle. The purple triangles indicate that for tilt GBs the grain rotation can be accomplished with little GB migration.

tion provide the first solid evidence that the grain rotation mechanism is strongly dependent on the type of GB. Because the GBs in a NC are usually of mixed types (see Fig. 1), the activation of GB dislocation activities, together with GB migration via atomic shuffling and disconnection activities, should be frequently observed. This is the mechanism at play for the general GBs during room-temperature grain rotation in NC metals.

4. Discussion

In the past decades, many classic grain rotation models were proposed. Li et al. [21,68] and Ovid'ko et al. [22] suggest that the grain rotation occurs via the absorption/generation, climb, and glide of inter-grain dislocations. These inter-grain dislocation activities leading to grain rotation only need short-range diffusion, and do not lead to obvious GB migration. While there are also many theoretical studies suggested that grain rotation needs long-range mass transport from compressive to tensile strained region, resulting in obvious GB migration. Previous theoretical model and MD simulation also proposed that grains can rotate via disconnection glide, with very small amount of long-range diffusion. Experimentally, some postmortem TEM examinations seem to support grain rotation via GB dislocations with negligible GB migration [28,31–34]. There are also many studies confirming that the GB migration plays an important role in grain rotation and growth [8–10]. The uncertainty makes us wonder how to reconcile these mechanisms, and determine the required experimental conditions. The results presented in this paper suggest that for the grains separated by mixed GBs, grains rotate through a combined activation of atomic shuffling, GB dislocation activities, and disconnection activities. Only when the grains are separated by a tilt GB, can the rotation be accomplished solely via the Frank–Bilby dislocation activities. As such, the current in situ experiments have straightened out the applicability among various models, by sorting out their respective validity limits.

Here, the GB dislocation interactions and climb at GB can lead to the formation and destruction of Lomer-lock-like structure at GB during rotation, which have not been reported in previous simulation and experiments. We also provide clear details about GB atomic shuffling, the absorption/generation, climb/glide and reaction of GB dislocation, as well as disconnection mediated GB migration during grain rotation. The current results are also different from previous TEM observation of grain rotation and coalescence via dislocations gliding away from GBs into the nanograins without GB migration [31,33,34,68]. Hence, our systematic TEM and MD work provides a more complete picture of grain rotation, which is much-needed to advance our understanding of the mechanical behavior of NC metals. It should be noted that previous studies dealt with different types of GBs, such that it is not surprising that both rotation mechanisms were frequently observed.

The grain rotation mechanisms revealed above are expected to be relevant to bulk NC samples. To make this projection, we can compare the effective GB diffusivity, D_g, in our thin film with that in bulk NC metals. D_g is a useful indicator because the dislocation climb is controlled by atomic diffusion. Comparing the thin film and bulk, a similar D_g would suggest that the same grain rotation mechanisms could be at play in both cases. In our experiments, the rotation angle and the time scale can be directly obtained from the TEM images, and then the average rotation rate can be calculated according to the formula $\frac{1}{n}\sum_{i=1}^{n}\frac{\Delta\theta_i}{t_i}$, where $\Delta\theta_i$ is the rotation angle and t_i is the corresponding time scale for this rotation. From Fig. 2, Fig. 6–Fig. 9, the measured $\Delta\theta_i$ are 8.6°, 13.9°, 4.0°, 2.0°, 7.4°, 3.8°, and the corresponding t_i are 9.5 s, 25 s, 5 s, 5 s, 15 s, 10 s respectively, then the average grain rotation rate, ω, is estimated to be $\sim 1.03 \times 10^{-2}$ rad/s (0.59°/s). To sustain such a rate, the required effective GB diffusivity can be derived from the phenomenological model for ω by Moldovan et al. [62,69]. It should be noted that a grain embedded in an NC metal is subjected to a torque that comes from the externally applied stress. According to a previous theoretical model [69], the torque is directly related to the externally applied stress and is given by

$$\omega = \frac{2\Omega T D_L}{\pi k T R_0^2 d \sum_{n=1}^{\infty} \frac{h_n^2+p_n^2}{\frac{1}{n}+\frac{\delta D_g}{2R_0 D_L}}} \tag{1}$$

where δ is the GB9- thickness, h_n and p_n the Fourier coefficients of the boundary shape, Ω the atomic volume, R_0 the average radius of the grain, d the column height (which is the same for each grain), k the Boltzmann constant, T the absolute temperature, D_L the self-diffusion coefficient for lattice diffusion, and T the torque acting on the grain with respect to its center.

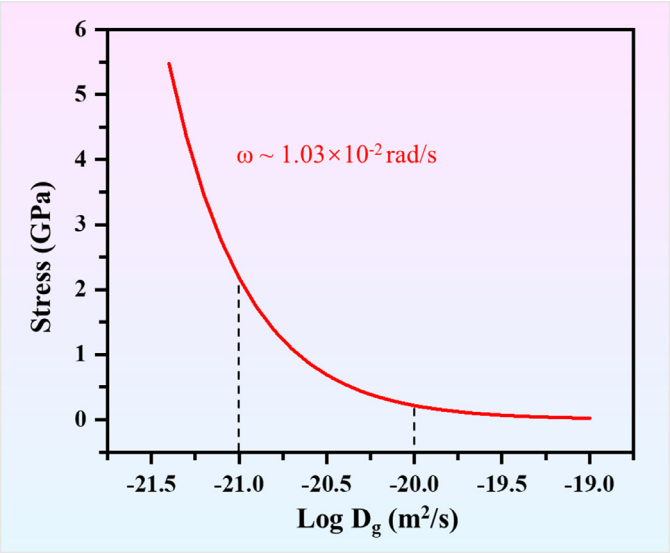

Fig. 13. The stress vs. logD_g , where D_g is the GB diffusion coefficient.

The torque (T) on the rotating grain is given by [69]

$$T = 2\pi d R_0^2 \tau, \tag{2}$$

where τ is the applied shear stress.

Considering $D_g \gg D_L$, and combining Eq. (1) and (2), we obtain

$$\omega = \frac{2\Omega\delta D_g \tau}{kTR_0 \sum_{n=1}^{\infty} \left(h_n^2 + p_n^2\right)}, \tag{3}$$

where R_0, h_n and p_n can be expressed as [69]

$$2R_0^2 + \sum_{n=1}^{\infty} \left(h_n^2 + p_n^2\right) = 1.654L^2. \tag{4}$$

Finally, the rotation rate equation becomes

$$\omega \approx \frac{2946 D_g \delta \Omega}{kTd^3} \tau. \tag{5}$$

Fig. 13 shows the stress versus GB diffusion coefficient based on Eq. (5). For the NC Pt in question, d ~10 nm ($\frac{d}{2} \approx 0.908L$ for grains with a hexagonal shape, where L is the length of the hexagon-shaped GB), δ = 0.5 nm, T= 353 K, and Ω = 15.6 × 10^{-30} m^3. According to the previous studies, the GB diffusion coefficient in NC metals is ~10^{-21} m^2/s [65,70–74] and the corresponding stress in Pt is estimated to be ~2.18 GPa, which is approximately 1.3% of the Young's modulus of Pt (168 GPa). The estimated stress/strain values, which are similar to those in a previous study, are required to trigger the GB plasticity in NC Cu [75] and Pd [76], are higher than that observed in NC Al (below ~ 0.5%) [77,78], and are smaller than that measured in NC Ni (in the range of 2.1%–5.5%) [79]. If we consider that the GB diffusion coefficient in an NC thin film is approximately ~10^{-20} m^2/s [65,80], then the corresponding stress in Pt is estimated to be ~0.22 GPa, which is only 0.13% of the Young's modulus of Pt, indicating that the GB mediated plasticity might be triggered more easily than that of bulk NC. This magnitude turns out to be close to the values measured in NC thin films of Al. The NC thin film with extremely large surface-to-volume ratio usually with higher diffusion coefficient [65], which can enhance the GB atomic diffusion, and thus lead to the GB diffusion coefficient of an NC thin film always higher than that of bulk NC metals. Previous studies also show that thin films could enhance atomic diffusion, dislocation nucleation, and climb [73,74,81] and may thus facilitate the grain rotation. Although the samples in our experiments are thin films, the observed rotation mechanism, to some extent, can also be extended to thick samples. For example, the GB migration accommodated by grain rotation was also observed in many thick samples [8,9,61,82]. The MD simulation [26,27] also confirmed that the grain rotation can still occur via GB migration and GB dislocation in both thin films and 3D NC samples. Based on this, we believe that our observed grain rotation mechanism may still occur in thick samples in experimental conditions, but it may require higher stress or smaller grain size. In addition, grain rotation is also important for super-plasticity [83] as well as the recrystallization in polycrystalline metals [18,21,83] at elevated temperatures. The grain rotation mechanisms we uncovered would also have important implications for understanding the GB-mediated plasticity in NC metals at elevated temperatures.

5. Conclusions

In conclusion, we have conducted in situ HRTEM straining experiments to reveal the atomic-scale processes accomplishing grain rotation in NC Pt at room temperature. Our work is focused on revealing the atomic-scale mechanisms of grain rotation at different types of GB, which have been rarely explored in experiments to date. For the first time, we clearly demonstrate that the grain rotation mechanism is dependent on the type of GB separating the rotating grains. Our findings resolve a longstanding uncertainty; actually both the Frank–Bilby dislocation activities and disconnection activities in conjunction with atomic shuffling are applicable to NC metals at room temperature, but the former predominates in tile GBs, while both are at work for the general case of mixed GBs. Besides, the formation and destruction of Lomer-like dislocations are a prevalent step inevitably encountered during the climb and reactions of GB dislocations. Our findings are based on a large number of in situ atomic-scale experiments on many mixed GBs, and should hence reflect the general behavior in NC metals.

Declaration of Competing Interest

The authors declare no competing interests.

Acknowledgements

This work was supported by the National Key R & D Program of China (2021YFA1200201); Beijing Natural Science Foundation (Z180014); the Beijing Outstanding Young Scientists Projects (BJJWZYJH01201910005018); the National Natural Science Foundation of China (No. 51771104, 91860202). E.M. acknowledges the support from the "111" project (DB18015) for hosting his research at BJUT.

Supplementary materials

Supplementary material associated with this article can be found, in the online version, at doi:10.1016/j.actamat.2022.118386.

References

[1] Z.T. Trautt, Y. Mishin, Grain boundary migration and grain rotation studied by molecular dynamics, Acta Mater. 60 (2012) 2407–2424.
[2] J. Schiotz, K.W. Jacobson, A maximum in the strength of nanocrystalline copper, Science 301 (2003) 1357–1359.
[3] V. Yamakov, D. Wolf, S.R. Phillpot, A.K. Mukherjee, H. Gleiter, Deformation-mechanism map for nanocrystalline metals by molecular dynamics simulation, Nat. Mater. 3 (2004) 43–47.
[4] M.A. Meyers, A. Mishra, D.J. Benson, Mechanical properties of nanocrystalline materials, Prog. Mater. Sci. 51 (2006) 427–556.
[5] Y.T. Zhu, X.Z. Liao, X.L. Wu, Deformation twinning in nanocrystalline materials, Prog. Mater. Sci. 57 (2012) 1–62.
[6] H. Van Swygenhoven, J.R. Weertman, Deformation in nanocrystalline metals, Mater. Today 9 (2006) 24–31.

[7] J.R. Greer, J.T.M. De Hosson, Plasticity in small-sized metallic systems: intrinsic versus extrinsic size effect, Prog. Mater. Sci. 56 (2011) 654–724.
[8] J.A. Sharon, P.C. Su, F.B. Prinz, K.J. Hemker, Stress-driven grain growth in nanocrystalline Pt thin films, Scripta Mater 64 (2011) 25–28.
[9] Z.W. Shan, E.A. Stach, W. Jmk, J.A. Knapp, D.M. Follstaedt, S.X. Mao, Grain boundary-mediated plasticity in nanocrystalline nickel, Science 305 (2004) 654–657.
[10] X.W. Gu, C.N. Loynachan, Z.X. Wu, Y.W. Zhang, D.J. Srolovitz, J.R. Greer, Size-dependent deformation of nanocrystalline Pt nanopillars, Nano Lett. 12 (2012) 6385–6392.
[11] P. Liu, S.C. Mao, L.H. Wang, X.D. Han, Z. Zhang, Direct dynamic atomic mechanisms of strain-induced grain rotation in nanocrystalline, textured, columnar-structured thin gold films, Scripta Mater 64 (2011) 343–346.
[12] M. Jin, A.M. Minor, E.A. Stach, J.W. Morris Jr, Direct observation of deformation-induced grain growth during the nanoindentation of ultrafine-grained Al at room temperature, Acta Mater 52 (2004) 5381–5387.
[13] B. Yang, H. Vehoff, A. Hohenwarter, M. Hafok, R. Pippan, Strain effects on the coarsening and softening of electrodeposited nanocrystalline Ni subjected to high pressure torsion, Scripta Mater 58 (2008) 790–793.
[14] B. Ratzker, A. Wagner, M. Sokol, S. Kalabukhov, N. Frage, Stress-enhanced dynamic grain growth during high-pressure spark plasma sintering of alumina, Acta Mater 164 (2019) 390–399.
[15] Y.J. Li, C.W. Hsu, Y.H. Ting, N.T. Tsou, Y.C. Lo, W.W. Wu, K.N. Tu, C. Chen, Deformation induced columnar grain rotation in nanotwinned metals, Mat. Sci. Eng. A 797 (2020) 140045.
[16] A. Dasgupta, P. Sharma, K. Upadhyayula, Micro-mechanics of fatigue damage in Pb-Sn solder due to vibration and thermal cycling, Int. J. Damage Mech. 10 (2001) 101–132.
[17] S.L. Thomas, K.T. Chen, J. Han, P.K. Purohit, D.J. Srolovitz, Reconciling grain growth and shear-coupled grain boundary migration, Nat. Commun. 8 (2017) 1764.
[18] D. Farkas, S. Mohanty, J. Monk, Linear grain growth kinetics and rotation in nanocrystalline Ni, Phys. Rev. Lett. 98 (2008) 165502.
[19] D. Wolf, V. Yamakov, S.R. Phillpot, A. Mukherjee, H. Gleiter, Deformation of nanocrystalline materials by molecular-dynamics simulation: relationship to experiments? Acta Mater 53 (2005) 1–40.
[20] E.R. Homer, S.M. Foiles, E.A. Holm, D.L. Olmsted, Phenomenology of shear-coupled grain boundary motion in symmetric tilt and general grain boundaries, Acta Mater 61 (2013) 1048–1060.
[21] J.C.M. Li, Mechanical grain growth in nanocrystalline copper, Phys. Rev. Lett. 96 (2006) 215506.
[22] I.A. Ovid'ko, A.G. Sheinerman, Special rotational deformation in nanocrystalline metals and ceramics, Scripta Mater 59 (2008) 119–122.
[23] F.C. Frank, in: Symposium on the Plastic Deformation of Crystalline Solids, Office of Naval Research, Pittsburgh, 1950, p. 150.
[24] B.A. Bilby, R. Bullough, E. Smith, Continuous distributions of dislocations: a new application of the methods of non-Riemannian geometry, Proc. R. Soc. Lond. A 231 (1955) 263–273.
[25] M.F. Ashby, R.A. Verrall, Diffusion-accommodated flow and superplasticity, Acta Metall. 21 (1973) 149–163.
[26] S. Kumar, X.Y. Li, A. Haque, H.J. Gao, Is stress concentration relevant for nanocrystalline metals? Nano Lett 11 (2011) 2510–2516.
[27] T. Shimokawa, A. Nakatani, H. Kitagawa, Mechanical properties depending on grain sizes of face-centered-cubic nanocrystalline metals using molecular dynamics simulation, JSME Int. J. Ser. A 47 (2004) 83–91.
[28] M. Murayama, J.M. Howe, H. Hidaka, S. Takaki, Atomic-level observation of disclination dipoles in mechanically milled, nanocrystalline Fe, Science 295 (2002) 2433–2435.
[29] J. Han, S.L. Thomas, D.J. Srolovitz, Grain-boundary kinetics: a unified approach, Prog. Mater. Sci. 98 (2018) 386–476.
[30] J.W. Cahn, J.E. Taylor, A unified approach to motion of grain boundaries, relative tangential translation along grain boundaries, and grain rotation, Acta Mater 52 (2004) 4887–4898.
[31] Y.B. Wang, J.C. Ho, X.Z. Liao, H.Q. Li, S.P. Ringer, Y.T. Zhu, Mechanism of grain growth during severe plastic deformation of a nanocrystalline Ni–Fe alloy, Appl. Phys. Lett. 94 (2009) 011908.
[32] L.H. Wang, J. Teng, P. Liu, A. Hirata, E. Ma, Z. Zhang, M.W. Chen, X.D. Han, Grain rotation mediated by grain boundary dislocations in nanocrystalline platinum, Nat. Commun. 5 (2014) 1–7.
[33] S. Ni, Y.B. Wang, X.Z. Liao, S.N. Alhajeri, H.Q. Li, Y.H. Zhao, E.J. Lavernia, S.P. Ringer, T.G. Langdon, Y.T. Zhu, Grain growth and dislocation density evolution in a nanocrystalline Ni–Fe alloy induced by high-pressure torsion, Scripta Mater 64 (2011) 327–330.
[34] J.Y. Huang, Y.T. Zhu, H.G. Jiang, T.C. Lowe, Microstructures and dislocation configurations in nanostructured Cu processed by repetitive corrugation and straightening, Acta Mater. 49 (2001) 1497–1505.
[35] L.H. Wang, X.D. Han, P. Liu, Y.H. Yue, Z. Zhang, E. Ma, In situ observation of dislocation behavior in nanometer grains, Phys. Rev. Lett. 105 (2010) 135501.
[36] S.D. Sun, D.W. Li, C.P. Yang, L.B. Fu, D.L. Kong, Y. Lu, Y.Z. Guo, D.M. Liu, P.F. Guan, Z. Zhang, J.H. Chen, W.Q. Ming, L.H. Wang, X.D. Han, Direct Atomic-Scale Observation of Ultrasmall Ag Nanowires that Exhibit fcc, bcc, and hcp Structures under Bending, Phys. Rev. Lett. 128 (2022) 015701.
[37] L.H. Wang, Y. Zhang, Z. Zeng, H. Zhou, J. He, P. Liu, M.W. Chen, J. Han, D.J. Srolovitz, J. Teng, Y.Z. Guo, G. Yang, D.L. Kong, E. Ma, Y.L. Hu, B.C. Yin, X.X. Huang, Z. Zhang, T. Zhu, X.D. Han, Tracking the sliding of grain boundaries at the atomic scale, Science 375 (2022) 1261–1265.
[38] Y. Amouyal, E. Rabkin, Y. Mishin, Correlation between grain boundary energy and geometry in Ni-rich NiAl, Acta Mater 53 (2005) 3795–3805.
[39] A. Morawiec, K. Glowinski, On "macroscopic" characterization of mixed grain boundaries, Acta Mater 61 (2013) 5756–5767.
[40] P. Hirel, Atomsk: a tool for manipulating and converting atomic data files, Comput. Phys. Commun. 197 (2015) 212–219.
[41] A. Stukowski, Visualization and analysis of atomistic simulation data with OVITO-the open visualization tool, Model. Simul. Mater. Sci. Eng. 18 (2010) 015012.
[42] S. Plimpton, Fast parallel algorithms for short-range molecular-dynamics, J. Comput. Phys. 117 (1995) 1–19.
[43] X.W. Zhou, R.A. Johnson, H.N.G. Wadley, Misfit-energy-increasing dislocations in vapor-deposited CoFe/NiFe multilayers, Phys. Rev. B 69 (2004) 144113.
[44] X.Y. Li, Y.J. Wei, W. Yang, H.J. Gao, Competing grain-boundary-and dislocation–mediated mechanisms in plastic strain recovery in nanocrystalline aluminum, Proc. Natl. Acad. Sci. USA 106 (2009) 16108–16113.
[45] D.A. Porter, K.E. Easterling, Phase Transformations in Metals and Alloys, 2nd Edition, CRC Press, 1992.
[46] H. Van Swygenhoven, P.M. Derlet, A. Hasnaoui, Atomic mechanism for dislocation emission from nanosized grain boundaries, Phys. Rev. B 66 (2002) 024101.
[47] V. Yamakov, D. Wolf, M. Salazar, S.R. Phillpot, H. Gleiter, Length-scale effects in the nucleation of extended dislocations in nanocrystalline Al by molecular–dynamics simulation, Acta Mater 49 (2001) 2713–2722.
[48] D. Rodney, R. Phillips, Structure and strength of dislocation junctions: an atomic level analysis, Phys. Rev. Lett. 82 (1999) 1704.
[49] R.W. Balluffi, Grain boundary diffusion mechanisms in metals, in: Metallurgical Transactions. A, Physical Metallurgy and Materials Science, 1982, pp. 2069–2095.
[50] J.J. Bean, K.P. McKenna, Origin of differences in the excess volume of copper and nickel grain boundaries, Acta Mater. 110 (2016) 246–257.
[51] V. Yamakov, D. Moldovan, K. Rastogi, D. Wolf, Relation between grain growth and grain-boundary diffusion in a pure material by molecular dynamics simulations, Acta Mater. 54 (2006) 4053–4061.
[52] M.R. Chellali, Z. Balogh, L. Zheng, G. Schmitz, Triple junction and grain boundary diffusion in the Ni/Cu system, Scripta Mater. 65 (2011) 343–346.
[53] M.R. Chellali, Z. Balogh, H. Bouchikhaoui, R. Schlesiger, P. Stender, L. Zheng, G. Schmitz, Triple junction transport and the impact of grain boundary width in nanocrystalline Cu, Nano Lett. 12 (2012) 3448–3454.
[54] Q. Zhu, G. Cao, J.W. Wang, C. Deng, J.X. Li, Z. Zhang, S.X. Mao, In situ atomistic observation of disconnection-mediated grain boundary migration, Nature Commun. 10 (2019) 1–8.
[55] A. Rajabzadeh, F. Mompiou, S. Lartigue-Korinek, N. Combe, M. Legros, D.A. Molodov, The role of disconnections in deformation-coupled grain boundary migration, Acta Mater. 77 (2014) 223–235.
[56] F. Mompiou, D. Caillard, M. Legros, Grain boundary shear–migration coupling—I. In situ TEM straining experiments in Al polycrystals, Acta Mater. 57 (2009) 2198–2209.
[57] A. Rajabzadeh, M. Legros, N. Combe, F. Mompiou, D.A. Molodov, Evidence of grain boundary dislocation step motion associated to shear-coupled grain boundary migration, Philos. Mag. 93 (2013) 1299–1316.
[58] P.M. Anderson, J.P. Hirth, J. Lothe, Theory of Dislocations, Cambridge Univ. Press, 2017.
[59] C.Y. Wang, K. Du, K.P. Song, X.L. Ye, L. Qi, S.Y. He, D.M. Tang, N. Lu, H.J. Jin, F. Li, H.Q. Ye, Size-dependent grain-boundary structure with improved conductive and mechanical stabilities in sub-10-nm gold crystals, Phy. Rev. Lett. 120 (2018) 186102.
[60] M.L. Bowers, C. Ophus, A. Gautam, F. Lancon, U. Dahmen, Step coalescence by collective motion at an incommensurate grain boundary, Phys. Rev. Lett. 116 (2016) 106102.
[61] A.J. Haslam, D. Moldovan, V. Yamakov, D. Wolf, S.R. Phillpot, H. Gleiter, Stress-enhanced grain growth in a nanocrystalline material by molecular-dynamics simulation, Acta Mater. 51 (2003) 2097–2112.
[62] K.E. Harris, V.V. Singh, A.H. King, Grain rotation in thin films of gold, Acta Mater. 46 (1998) 2623–2633.
[63] T. Zhu, J. Li, Ultra-strength materials, Prog. Mater. Sci. 55 (2010) 710–757.
[64] L. Sun, F. Banhart, A.V. Krasheninnikov, J.A. Rodriǵuez-manzo, M. Terrones, P.M. Ajayan, Carbon nanotubes as high-pressure cylinders and nanoextruders, Science 312 (2006) 1199–1202.
[65] I. Kaur, Y. Mishin, W. Gust, Fundamentals of Grain and Interphase Boundary Diffusion, Wiley & Sons, Chichester, UK, 1995.
[66] J. Wang, R.G. Hoagland, A. Misra, Room-temperature dislocation climb in metallic interfaces, Appl. Phys. Lett. 94 (2009) 131910.
[67] H. Van Swygenhoven, P.M. Derlet, Grain-boundary sliding in nanocrystalline fcc metals, Phys. Rev. B 64 (2001) 224105.
[68] J.C.M. Li, Possibility of subgrain rotation during recrystallization, J. Appl. Phys. 33 (1962) 2958–2965.
[69] D. Moldovan, D. Wolf, S.R. Phillpot, Theory of diffusion-accommodated grain rotation in columnar polycrystalline microstructures, Acta Mater 49 (2001) 3521–3532.
[70] W. Gust, S. Mayer, A. Bögel, B. Predel, Generalized representation of grain boundary self-diffusion data, J. Physique 46 (1985) 537–544.
[71] R. Würschum, S. Herth, U. Brossmann, Diffusion in nanocrystalline metals and alloys-A status report, Adv. Eng. Mater. 5 (2003) 365–372.
[72] B. Cai, Q.P. Kong, L. Lu, K. Lu, Low temperature creep of nanocrystalline pure copper, Mater. Sci. Eng. A 286 (2000) 188–192.

[73] D.S. Gianola, D. Farkas, M. Gamarra, M.R. He, The role of confinement on stress-driven grain boundary motion in nanocrystalline aluminum thin films, J. Appl. Phys. 112 (2012) 124313.
[74] F. Mompiou, M. Legros, A. Boé, M. Coulombier, J.-P. Raskin, T. Pardoen, Inter- and intragranular plasticity mechanisms in ultrafine-grained Al thin films: an in situ TEM study, Acta Mater. 61 (2013) 205–216.
[75] J. Schiøtz, F.D. Di Tolla, K.W. Jacobsen, Softening of nanocrystalline metals at very small grain sizes, Nature 391 (1998) 561–563.
[76] K. Yang, H.J. Fecht, Y. Ivanisenko, First direct in situ observation of grain boundary sliding in ultrafine grained noble metal, Adv. Eng. Mater. 16 (2014) 517–521.
[77] T.J. Rupert, D.S. Gianola, Y. Gan, K.J. Hemker, Experimental observations of stress-driven grain boundary migration, Science 326 (2009) 1686–1690.
[78] D.S. Gianola, S. Van Petegem, M. Legros, S. Brandstetter, H. Van Swygenhoven, K.J. Hemker, Stress-assisted discontinuous grain growth and its effect on the deformation behavior of nanocrystalline aluminum thin films, Acta Mater. 54 (2006) 2253–2263.
[79] Z.W. Shan, J.M.K. Wiezorek, J.A. Knapp, D.M. Follstaedt, E.A. Stach, S.X. Mao, Large lattice strain in individual grains of deformed nanocrystalline Ni, Appl. Phys. Lett. 92 (2008) 091917.
[80] M. DiBattista, J.W. Schwank, Determination of diffusion in polycrystalline platinum thin films, J. Appl. Phys. 86 (1999) 4902–4907.
[81] P.M. Derlet, H.V. Swygenhoven, The role played by two parallel free surfaces in the deformation mechanism of nanocrystalline metals: a molecular dynamics simulation, Philos. Mag. A 82 (2002) 1–15.
[82] X.Z. Liao, A.R. Kilmametov, R.Z. Valiev, H.S. Gao, X.D. Li, A.K. Mukherjee, J.F. Bingert, Y.T. Zhu, Deformationinduced grain rotation and growth in nanocrystalline Ni, Appl. Phys. Lett. 88 (2006) 021909.
[83] F.J. Humphreys, M. Hatherly, Recrystallization and Related Annealing Phenomena, Elsevier Science, Oxford, UK, 1995.